

Histone lysine methyltransferase Pr-set7/SETD8 promotes neural stem cell reactivation

Jiawen Huang¹ , Mahekta R Gujar¹, Qiannan Deng¹, Sook Y Chia^{1,†}, Song Li¹, Patrick Tan^{2,3,4,5}, Wing-Kin Sung^{2,6} & Hongyan Wang^{1,7,8,*} 

Abstract

The ability of neural stem cells (NSCs) to switch between quiescence and proliferation is crucial for brain development and homeostasis. Increasing evidence suggests that variants of histone lysine methyltransferases including KMT5A are associated with neurodevelopmental disorders. However, the function of KMT5A/Pr-set7/SETD8 in the central nervous system is not well established. Here, we show that *Drosophila* Pr-Set7 is a novel regulator of NSC reactivation. Loss of function of *pr-set7* causes a delay in NSC reactivation and loss of H4K20 monomethylation in the brain. Through NSC-specific *in vivo* profiling, we demonstrate that Pr-set7 binds to the promoter region of *cyclin-dependent kinase 1 (cdk1)* and Wnt pathway transcriptional co-activator *earthbound1/jerky (ebd1)*. Further validation indicates that Pr-set7 is required for the expression of *cdk1* and *ebd1* in the brain. Similar to Pr-set7, Cdk1 and Ebd1 promote NSC reactivation. Finally, overexpression of Cdk1 and Ebd1 significantly suppressed NSC reactivation defects observed in *pr-set7*-depleted brains. Therefore, Pr-set7 promotes NSC reactivation by regulating Wnt signaling and cell cycle progression. Our findings may contribute to the understanding of mammalian KMT5A/PR-SET7/SETD8 during brain development.

Keywords *Drosophila*; neural stem cell; Pr-set7; quiescence; reactivation

Subject Categories Chromatin, Transcription & Genomics; Neuroscience; Stem Cells & Regenerative Medicine

DOI 10.15252/embr.202050994 | Received 29 May 2020 | Revised 5 January 2021 | Accepted 12 January 2021 | Published online 10 February 2021

EMBO Reports (2021) 22: e50994

Introduction

Stem cells have the ability to undergo proliferation, differentiation, and quiescence. The balance between these states is crucial for

neurogenesis and regeneration. In the adult mammalian brains, most neural stem cells (NSCs) remain in quiescence, a mitotically dormant state (Morshead *et al*, 1994; Doetsch *et al*, 1999). Quiescent NSCs can re-enter cell cycle (termed reactivation) to generate new neurons in response to various physiological stimuli, such as injury, the presence of nutrients, and physical exercise (Ahn & Joyner, 2005; Lugert *et al*, 2010; Wang *et al*, 2011; Daynac *et al*, 2013; Faiz *et al*, 2015; Daynac *et al*, 2016; Kawai *et al*, 2017; Otsuki & Brand, 2017, 2020; Ding *et al*, 2020). Conversely, the proliferation capacity of NSCs is greatly reduced upon stress, anxiety, and old age (Lucassen *et al*, 2010). Dysregulation of NSC quiescence and reactivation would severely affect tissue homeostasis. While excessive reactivation depletes NSC pools, failure of reactivation leads to defects in neurogenesis (Cheung & Rando, 2013; Braun & Jessberger, 2014). Therefore, it is of great importance to understand the mechanisms controlling the NSC quiescence and reactivation.

Drosophila larval brain NSCs, also known as neuroblasts, have emerged as an excellent *in vivo* model to study molecular mechanisms underlying NSC quiescence and reactivation. At the end of embryogenesis, *Drosophila* NSCs in the central nervous system shrink in size and enter quiescence (Truman & Bate, 1988; Ito & Hotta, 1992; Britton & Edgar, 1998). The quiescence entry is regulated by a combined function of temporal identity factors, the spatial control homeobox genes, and a homeodomain differentiation factor Prospero (Pros; Isshiki *et al*, 2001; Tsuji *et al*, 2008; Lai & Doe, 2014; Otsuki & Brand, 2019). Notably, only 25% of quiescent NSCs arrest in the G₀ stage, while the majority of quiescent NSCs (75%) are in the G₂ stage (Otsuki & Brand, 2018). Quiescent NSCs extend their primary protrusions toward the neuropil until they begin to divide (Truman & Bate, 1988; Tsuji *et al*, 2008; Chell & Brand, 2010) and appear to use this microtubule enriched structure to directly contact the neuropil (Deng *et al*, 2020). After about 24 h, quiescent NSCs re-enter the cell cycle to resume neurogenesis in response to feeding (Truman & Bate, 1988; Ito & Hotta, 1992; Britton & Edgar, 1998). During the reactivation, NSCs appear to lose the protrusion

1 Neuroscience & Behavioral Disorders Programme, Duke-NUS Medical School, Singapore, Singapore

2 Genome Institute of Singapore, Singapore, Singapore

3 Cancer & Stem Cell Biology Program, Duke-NUS Medical School, Singapore, Singapore

4 Cellular and Molecular Research, National Cancer Centre, Singapore, Singapore

5 Cancer Science Institute of Singapore, National University of Singapore, Singapore, Singapore

6 Department of Computer Science, National University of Singapore, Singapore, Singapore

7 Department of Physiology, Yong Loo Lin School of Medicine, National University of Singapore, Singapore, Singapore

8 Integrative Sciences and Engineering Programme, National University of Singapore, Singapore, Singapore

*Corresponding author. Tel: +65 65167740; E-mail: hongyan.wang@duke-nus.edu.sg

†Present address: National Neuroscience Institute, Singapore, Singapore

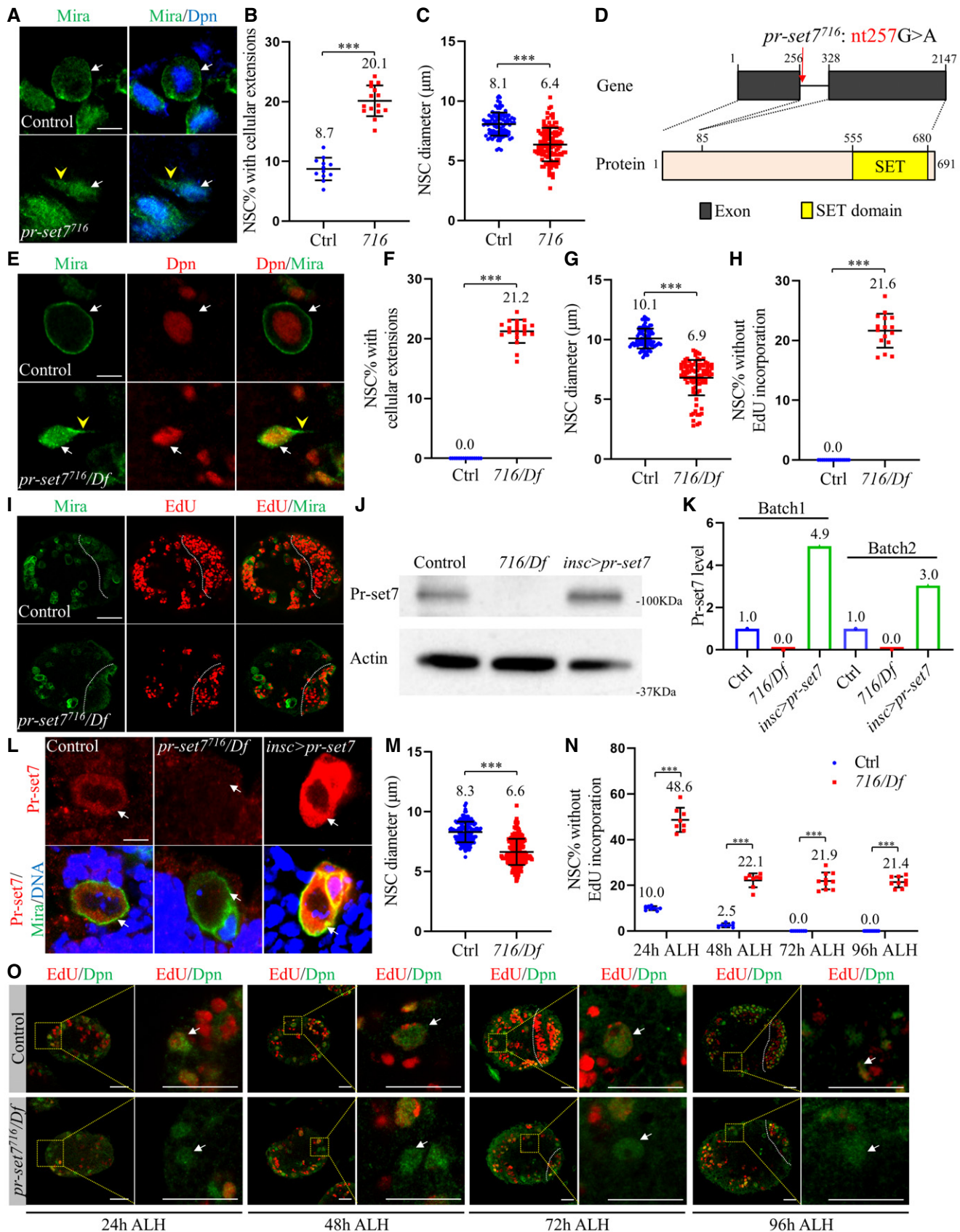


Figure 1.

Figure 1. Pr-set7 is required for NSC reactivation.

- A Larval NSCs of control (ctrl; *yw*) and *pr-set7⁷¹⁶* (716) at 24 h ALH were stained for Deadpan (Dpn) and Miranda (Mira).
- B, C Quantifications of cellular extensions (B) and NSC diameters (C) for genotypes in (A). In (B), $n = 1055$, 12 brain lobes [BL] for control; $n = 1000$, 15 BL for *pr-set7⁷¹⁶*. In (C), $n = 101$ for control; $n = 112$ for *pr-set7⁷¹⁶*.
- D A schematic representation of the *pr-set7⁷¹⁶* mutation. *pr-set7⁷¹⁶* contains a G to A point mutations at 831 nucleotides (nt). *Drosophila* Pr-set7 contains a SET domain (in yellow), which is required for its methyl transferase activity.
- E Larval NSCs of control (ctrl; *yw*) and *pr-set7⁷¹⁶/Df(3R)ED5644* (716/Df) at 96 h ALH were labeled with Dpn and Mira.
- F, G Quantifications of cellular extensions (F) and NSC diameters (G) for genotypes in (E). In (F), $n = 1488$, 15 BL for control; $n = 2014$, 20 BL for *pr-set7⁷¹⁶/Df*. In (G), $n = 92$ for control; $n = 93$ for *pr-set7⁷¹⁶/Df*.
- H Quantifications of EdU incorporation for genotypes in (I). Control, $n = 1365$, 16 BL; *pr-set7⁷¹⁶/Df*, $n = 1006$, 16 BL.
- I Larval brains of control (ctrl; *yw*) and *pr-set7⁷¹⁶/Df* at 96 h ALH were labeled with Dpn and EdU.
- J, K Western blot and quantification analysis of larval brain extracts of control (ctrl; *yw*), *pr-set7⁷¹⁶/Df*, and UAS-*pr-set7* induced with *insc-Gal4* at 72 h ALH ($n = 2$ as biological replicates). Blots were probed with anti-Pr-set7 antibody or anti-Actin antibody (loading control). Pr-set7 levels were normalized against actin intensity.
- L Larval NSCs of control (ctrl; *yw*), *pr-set7⁷¹⁶/Df*, and UAS-*pr-set7* induced with *insc-Gal4* at 72 h ALH were stained for Pr-set7, Mira, and DNA.
- M, N Quantifications of NSC diameters (M) at 24 h ALH and EdU incorporation (N) for genotypes in (O). In (M), $n = 152$ for control; $n = 129$ for *pr-set7⁷¹⁶/Df*. In (N), control, $n = 601$, 13 BL at 24 h ALH; $n = 988$, 14 BL at 48 h ALH; $n = 813$, 9 BL at 72 h ALH and $n = 829$, 10 BL at 96 h ALH. For *pr-set7⁷¹⁶/Df*, $n = 566$, 12 BL at 24 h ALH; $n = 808$, 13 BL at 48 h ALH; $n = 1032$, 10 BL at 72 h ALH and $n = 825$, 9 BL at 96 h ALH.
- O Larval brains of control (ctrl; *yw*) and *pr-set7⁷¹⁶/Df* at 24, 48, 72, and 96 h ALH were labeled with Dpn and EdU.

Data information: Quantification data are presented in as mean \pm SD (B, C, F, G, H, M, N). n numbers in (B, F, H, N) were total NSCs counted with total brain lobes measured, while each brain lobe considered as one biological replicate. Yellow dotted boxes indicate the region of zoomed-in images (O). White arrows point to NSCs and yellow arrowheads point to cellular extensions of NSCs. The central brain is to the left of white dotted lines (I, O). Statistical analyses were done comparing two different genotypes using Mann–Whitney test (B, C, F, G, H, M, N). *** $P < 0.001$. Scale bars, 5 μ m (A, E, L), 15 μ m (O), 30 μ m (I). Source data are available online for this figure.

either through retraction (Otsuki & Brand, 2018) or by segregating the protrusion into the ganglion mother cell following their first asymmetric division (Bostock *et al*, 2020). Dietary amino acids are sensed by the fat body, functional equivalence of mammalian liver, and adipose tissue (Colombani *et al*, 2003), which signals blood–brain barrier (BBB) glial cells to produce and secrete insulin-like peptides (dILPs) dILP2 and dILP6. dILPs diffuse directly to the underlying NSCs, activate the insulin/PI3K/Akt pathway, and drive NSC reactivation (Britton & Edgar, 1998; Chell & Brand, 2010; Sousa-Nunes *et al*, 2011; Speder & Brand, 2014). In mammalian brains, insulin-like growth factor (IGF-1) produced by astroglial cells acts locally to promote NSC proliferation in response to brain injury (Ye *et al*, 2004; Yan *et al*, 2006; Mairet-Coello *et al*, 2009). Besides the insulin/PI3K/Akt pathway, the Hippo pathway maintains NSC quiescence by inactivating Yorkie (Ding *et al*, 2016; Poon *et al*, 2016). This pathway is inactivated in response to dietary amino acids and is negatively regulated by an E3 ubiquitin ligase CRL4^{Mahj} (Ly *et al*, 2019). Furthermore, NSC reactivation also requires intrinsic factors including spindle matrix proteins Chromator (Li *et al*, 2017), Hsp83/Hsp90 (Huang & Wang, 2018), striatin-interacting phosphatase and kinase (STRIPAK) family proteins (Gil-Ranedo *et al*, 2019), and Mini spindles-dependent microtubule growth (Deng *et al*, 2020).

KMT5A/Pr-set7/SETD8 is the sole histone H4 Lys 20 monomethyltransferase (H4K20me1) (Nishioka *et al*, 2002). Pr-set7 and H4K20me1 play critical roles in maintaining genome stability, DNA repair and replication, cell cycle regulation, and chromatin compaction (Beck *et al*, 2012). Although H4K20me1 has been extensively studied as an epigenetic mark, its function in gene regulation remains uncertain, as it correlates with both gene expression and repression (Nishioka *et al*, 2002; Karachentsev *et al*, 2005; Trojer *et al*, 2007; Oda *et al*, 2009). Pr-set7/H4K20me1 can, directly and indirectly, promote chromatin condensation (Trojer *et al*, 2007; Oda *et al*, 2009) and loss of *pr-set7* suppresses the variegation phenotype in *Drosophila*, indicating the role of Pr-set7 functions as a gene

silencer (Karachentsev *et al*, 2005). On the other hand, genome-wide analysis reveals that Pr-set7 and H4K20me1 highly correlate with transcriptional activation (Talasiz *et al*, 2005; Vakoc *et al*, 2006; Barski *et al*, 2007; Wang *et al*, 2008; Cui *et al*, 2009; Wakabayashi *et al*, 2009). Increasing evidence suggests that variants of histone lysine methyltransferases including KMT5A are associated with neurodevelopmental disorders (Wickramasekara & Stessman, 2019). However, the function of KMT5A/Pr-set7/SETD8 in the central nervous system is not well established.

Here, we show that *Drosophila* Pr-set7 is required for NSC reactivation through regulating Wnt signaling and cell-cycle progression. Loss of *pr-set7* results in defects of NSC reactivation including failure to incorporate EdU and retaining their cellular extensions. Moreover, H4K20me1 was lost in *pr-set7*-depleted larval brains. Through targeted DNA adenine methyltransferase (Dam) identification (TaDa)-based *in vivo* profiling, we demonstrate that Pr-set7 binds to the promoter region of cell-cycle regulator *cdk1* and Wnt pathway transcriptional and co-activator *earthbound1/Jerky (Ebd1)* in NSCs. Further *in vivo* analysis indicates that Pr-set7 promotes the expression of Cdk1 and Ebd1 in NSCs. Finally, overexpression of Cdk1 and Ebd1 significantly suppresses reactivation defects resulted from *pr-set7* loss of function. Therefore, Pr-set7 promotes the expression of cell-cycle regulator Cdk1 and Wnt Signaling pathway.

Results

Isolation of *pr-set7* loss-of-function allele with NSC reactivation defects

To identify novel regulators of NSC reactivation and homeostasis, we carried out a genetic screen on chromosome 3R in a collection of ethyl methane sulfonate (EMS)-induced mutations (Ly *et al*, 2019) and isolated a new allele of *pr-set7*, *pr-set7⁷¹⁶*. At 24 h ALH, the majority of control NSCs were reactivated with a diameter of

8.1 ± 1.0 μm (Fig 1A and C), and only 8.7 ± 1.9% of NSCs retained cellular extensions (Fig 1A and B). However, at 24 h ALH the NSC diameter of *pr-set7⁷¹⁶* was 6.4 ± 1.4 μm (Fig 1A and C) and 20.1 ± 2.6% of NSCs exhibited cellular extensions (Fig 1A and B). These observations suggested that *pr-set7⁷¹⁶* NSCs displayed defects in NSC reactivation. Genetic mapping and molecular sequencing experiments indicated that *Pr-set7⁷¹⁶* contained a point mutation (nucleotides # 257 G to A) at the splice donor site in the intron, presumably resulting in a truncated *pr-set7* due to retaining of the intron that contains a premature stop codon (TAG) at 282 nucleotides (Fig 1D). *Drosophila* Pr-set7 contains a conserved SET domain that is responsible for its methyl transferase activity, at the carboxyl-terminus (Fig 1D) (Brustel et al, 2011). *pr-set7⁷¹⁶* might lose its methyl transferase function as a result of the putative truncation. Homozygous *pr-set7⁷¹⁶* larvae are semi-lethal at the early larval stage, with few survived to the second instar larval stage, presumably due to additional mutations in this strain. To eliminate the effect of a potential second-site mutation in *pr-set7⁷¹⁶*, we examined hemizygotes *pr-set7⁷¹⁶/Df(3R)ED5644* (BDSC#9090), which survived to late third instar stages. At 96 h after larval hatching (ALH), all NSCs in the central brain showed round morphology without cellular extensions, indicating that all of them were reactivated (Fig 1E and F). However, at this time point, there were still 21.2 ± 1.9% of NSCs from hemizygous *pr-set7⁷¹⁶/Df(3R)ED5644* displayed cellular extensions (Fig 1E and F). At 96 h ALH, all NSCs (Fig 1H and I) were proliferative and incorporated 5-ethynyl-2'-deoxyuridine (EdU). By contrast, 21.6 ± 2.8% of *pr-set7⁷¹⁶/Df(3R)ED5644* NSCs failed to incorporate EdU at 96 h ALH (Fig 1H and I). These observations suggested that *pr-set7* mutant NSCs failed to reactivate even at late larval stages. Consistent with these observations, at 24 h ALH, the NSC diameter of hemizygous *pr-set7⁷¹⁶/Df(3R)ED5644* (Fig 1M; 6.6 ± 1.1 μm) was much smaller than that of control NSCs (Fig 1M; 8.3 ± 0.9 μm). Moreover, at 96 h ALH, the size of *pr-set7⁷¹⁶/Df(3R)ED5644* NSCs remained much smaller (Fig 1G, 6.8 ± 1.5 μm) than that of control NSCs (Fig 1G, 10.1 ± 0.8 μm). These observations indicate that a significant number of NSCs failed to exit quiescence even at late larval stages upon loss of *pr-set7*. We generated anti-Pr-set7 antibodies against its 412-691 aa at the C-terminal region including the SET domain and detected Pr-set7 protein at the predicted size of 100 kDa in control larval brain extracts (Fig 1J; Karachentsev et al, 2005). Pr-set7 levels in Western blot were reduced to 0% in hemizygous *pr-set7⁷¹⁶/Df(3R)ED5644* larval brains at 72 h ALH (Fig 1K). Furthermore, Pr-set7 detected by immunostaining in control NSCs was completely absent in hemizygous *pr-set7⁷¹⁶/Df(3R)ED5644* larval brains (Fig 1L). These observations indicate that *pr-set7⁷¹⁶* appears to generate a truncation without its SET domain. Therefore, *pr-set7⁷¹⁶/Df(3R)ED5644* is likely a strong loss-of-function allele without methyltransferase activity. Therefore, we used *pr-set7⁷¹⁶/Df(3R)ED5644*, which was referred to as *pr-set7* mutant, for most of our subsequent analyses in this study. We examined the *pr-set7* heterozygous larval brains (*pr-set7⁷¹⁶/+*) and found that it had no NSC reactivation defects and was indistinguishable from the “wild-type” control *yw* (Fig EV1A and B). Therefore, *yw* is used as a control throughout this study.

Next, we examined other allelic combinations among *pr-set7⁷¹⁶*, other putative loss-of-function alleles of *pr-set7* or *Df(3R)ED5644*. *pr-set7^{EY04668}* (BDSC#15761) contains a P-element insertion at the 3'UTR, 1023 bp downstream of the stop codon (Bellen et al, 2004), while in *pr-set7^{M108086}* (BDSC#44742) a P-element is inserted 394 bp upstream

of start codon (Venken et al, 2011). Consistently, all other trans-heterozygotes or hemizygotes of *pr-set7* mutant alleles we have tested displayed similar NSC reactivation defects. At 24 h ALH, almost all wild-type control NSCs were reactivated with only 7.5 ± 1.8% of NSCs exhibited cellular extension (Fig EV1C and D). However, in *pr-set7^{EY04668}/Df(3R)ED5644* (17.2 ± 1.3%), *pr-set7^{EY04668}/pr-set7⁷¹⁶* (17.6 ± 2.0%), *pr-set7^{M108086}/Df(3R)ED5644* (19.4 ± 4.3%), and *pr-set7^{M108086}/pr-set7⁷¹⁶* (16.2 ± 3.1%), significantly more NSCs still retained cellular extensions at 24 h ALH (Fig EV1C and D).

To further validate the role of Pr-set7 in NSC reactivation, we generated transgenic UAS-Pr-set7 expressing a full-length Pr-set7. At 72 h ALH at 29°C, all control NSCs was reactivated without cellular extensions (Fig EV1E and F) and they all incorporated EdU (Fig EV1G and I). At the same condition, 18.5 ± 2.4% of *pr-set7* NSCs showed cellular extensions (Fig EV1E and F). Similarly, 18.8 ± 2.1% of NSCs with hemizygous *pr-set7* were EdU-negative at the same stage (Fig EV1G and I). Expression of *pr-set7* under *insc-Gal4* partially rescued the reactivation defects observed in *pr-set7* NSCs at 72 h ALH at 29°C; cellular extensions were only observed in 7.4 ± 2.0% of NSCs (Fig EV1E and F) and only 5.4 ± 3.0% of NSCs failed to incorporate EdU (Fig EV1G and I). This partial rescue was likely due to insufficient expression level of Pr-set7 in quiescent NSCs under *insc-Gal4*. Therefore, we generated a genomic rescue construct “*pr-set7* BAC”, using CH322-129L5, a 19.3 kb bacterial artificial chromosome (BAC) containing the *pr-set7* gene region and its regulatory elements. *pr-set7*-BAC essentially rescued NSC reactivation defects of *pr-set7* mutant; Almost all *pr-set7* NSCs with *pr-set7*-BAC were reactivated, with only 1.1 ± 1.4% (Fig EV1E and F) of them displayed cellular extensions and 2.1 ± 2.2% (Fig EV1G and I) of them lacked EdU incorporation. Taken together, these results indicate that Pr-set7 is required for NSC reactivation.

To further monitor at which stage Pr-set7 is required for NSC reactivation, we performed the time-course analysis at 24, 48, 72, and 96 h ALH. At 24 h ALH, the vast majority of control NSCs were reactivated and only 5.1 ± 0.9% of NSCs contained cellular extensions (Fig EV1H and J). By contrast, 25.8 ± 1.9% of *pr-set7* NSCs possessed cellular extensions at the same time point (Fig EV1H and J). Consistently, at 24 h ALH, most control NSCs re-entered the cell cycle, with only 10.0 ± 0.9% of them lacking EdU incorporation (Fig 1N and O). In comparison, 48.6 ± 5.3% of *pr-set7* NSCs failed to incorporate EdU at 24 h ALH (Fig 1N and O). This finding suggests that loss of *pr-set7* impairs NSC reactivation at the early larval stage. At 48 h ALH, nearly all control NSCs were reactivated, as only 0.2 ± 0.3% (Fig EV1H and J) of them retained cellular extensions and 2.5 ± 0.9% (Fig 1N and O) were EdU-negative. By contrast, cellular extensions and failure of EdU incorporation were observed in 18.2 ± 2.1% (Fig EV1H and J) and 22.1 ± 3.1% (Fig 1N and O) of *pr-set7* NSCs, respectively. At 72 h and 96 h ALH, all control NSCs lost cellular extensions (Fig EV1H and J) and incorporated with EdU (Fig 1N and O). However, even at late larval stages, a significant portion of *pr-set7* NSCs still exhibited cellular extensions, with 17.7 ± 0.9% at 72 h ALH and 20.4 ± 0.9% at 96 h ALH (Fig EV1H and J). Similarly, 21.9 ± 3.7% and 21.4 ± 2.4% of *pr-set7* NSCs lacked EdU incorporation at 72 h and 96 h ALH, respectively (Fig 1N and O).

To confirm that Pr-set7 functions in the NSCs, we knocked down *pr-set7* in NSCs under the control of *insc-Gal4*, an NSC-specific driver. At 24 hours ALH at 29°C, 16.0 ± 3.3% (Fig EV1K and L) of

control NSCs lacked EdU incorporation. By contrast, *pr-set7* RNAi (NIG #3307R-3) under *insc*-Gal4 resulted in a failure to incorporate EdU in $33.0 \pm 5.6\%$ (Fig EV1K and L) of NSCs at the same condition. This indicates that Pr-set7 could function in NSCs to promote their reactivation. Furthermore, total NSC numbers per brain lobe in control (75.2 ± 5.4 , $n = 13$ BL) and *pr-set7⁷¹⁶/Df* brains (77.9 ± 7.0 , $n = 13$ BL) at 48 h ALH were similar, suggesting that NSC survival is unlikely affected in the *pr-set7* mutant. When *pr-set7* was overexpressed under *insc*-Gal4 at 6 h ALH at 29°C, $15.5 \pm 3.0\%$ incorporated EdU, similar to that of control NSCs (Fig EV1M and N; $15.6 \pm 1.6\%$). Therefore, Pr-set7 overexpression could not induce precocious cell-cycle re-entry.

Taken together, Pr-set7 is required for the initiation of NSC reactivation.

Pr-set7 levels increase along with NSC reactivation

Given that Pr-Set7 is required for NSC reactivation, we examined the expression pattern of Pr-set7 in the larval brain in a time-course analysis. At 0 h ALH, the level of Pr-set7 in control brains was nearly absent and increased significantly at 24 h ALH and 48 h ALH (Fig 2A and B). Pr-set7 was observed mainly in the cytoplasm in NSCs, probably due to the low amount of Pr-set7 in the nucleus of NSCs. This observation is consistent with previous findings that Pr-

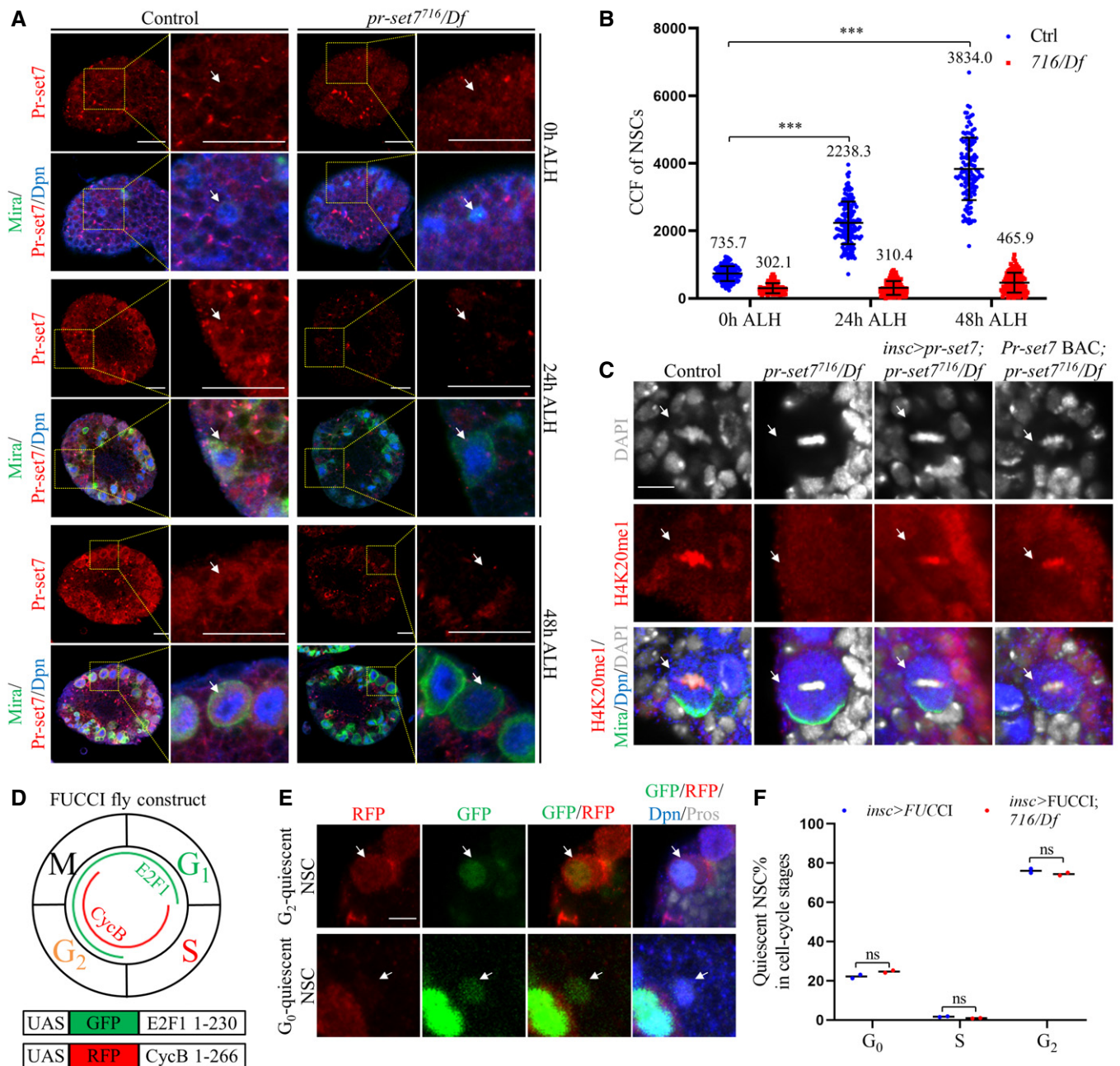


Figure 2.

Figure 2. Pr-set7 levels increase with NSC reactivation and is required for H4K20me1 in larval brains.

- A Larval NSCs of control (ctrl; *yw*) and *pr-set7⁷¹⁶/Df(3R)ED5644 (716/Df)* at 0, 24 and 48 h ALH were stained for Pr-set7, Dpn, and Mira. Yellow dotted boxes, zoomed-in area.
- B Quantifications of the corrected total cell fluorescence (CCF) for genotypes in (A). CCF = Integrated Density – (area of selected cell × mean fluorescence of background readings). At 0 h ALH, CCFs were 735.7 ± 220.7 (*n* = 168) for control, 302.1 ± 150.0 (*n* = 160) for 716/Df. At 24 h ALH, CCFs were 2238.3 ± 628.4 (*n* = 158) for control, 310.4 ± 207.1 (*n* = 113) for 716/Df. At 48 h ALH, CCFs were 3834.0 ± 924.2 (*n* = 124) for control, 465.9 ± 295.0 (*n* = 126) for 716/Df. Data are presented as mean ± SD. Statistical analyses were done comparing between the CCFs at later time points with the CCFs for control at 0 h ALH using Mann–Whitney test. ****P* < 0.001.
- C Larval NSCs of control (ctrl; *yw*), *pr-set7⁷¹⁶/Df*, *pr-set7⁷¹⁶/Df* with UAS-*pr-set7* induced with *insc-Gal4*, and *pr-set7⁷¹⁶/Df* with *pr-set7*-BAC at 24 h ALH were stained for H4K20me1, Dpn, Mira, and DAPI. Control: *n* = 108; *pr-set7⁷¹⁶/Df*: *n* = 87; *pr-set7⁷¹⁶/Df* with UAS-*pr-set7* induced with *insc-Gal4*: *n* = 167 and *pr-set7⁷¹⁶/Df* with *pr-set7*-BAC: *n* = 104.
- D A schematic representation of the FUCCI.
- E Larval NSCs with FUCCI constructs induced with *insc-Gal4* at 24 h were stained for GFP, RFP, Dpn, and Prospero (Pros).
- F Quantifications of quiescent NSCs in different cell-cycle stages from FUCCI flies (induced with *insc-Gal4*) in control (and *insc-Gal4* > FUCCI) and *pr-set7⁷¹⁶/Df*. Quiescent NSCs of *insc-Gal4* > FUCCI: 76.1 ± 1.5% in G₂, 1.7 ± 0.2% in S and 22.2 ± 1.3% in G₀ (*n* = 343). Quiescent NSCs of *insc-Gal4* > FUCCI; *pr-set7⁷¹⁶/Df*: 74.4 ± 1.0% in G₂, 0.9 ± 0.2% in S and 24.7 ± 0.8% in G₀ (*n* = 344).
- Data information: Quantification data are presented in as mean ± SD (B, F). Statistical analyses were done comparing two different genotypes using Mann–Whitney test (B, F). ns: non-significant. White arrows point to NSCs. Scale bars, 5 μm (C, E), 15 μm (A).

set7 contains a nuclear localization signal (NLS) and displays both cytoplasmic and nuclear localization in *Drosophila* S2 cells (Zouaz et al, 2018). Pr-set7 was undetectable in *pr-set7* mutant NSCs at both 24 h ALH and 48 h ALH (Fig 2A and B). As shown earlier, Pr-set7 was absent in *pr-set7* mutant NSCs at 72 h ALH, while it was upregulated upon Pr-set7 overexpression in the brain (Fig 1L), indicating that the anti-Pr-set7 antibodies were specific. These observations suggest that Pr-set7 levels increase along with NSC reactivation.

H4K20 monomethylation is lost in *pr-set7* mutant NSCs

Pr-Set7, essential for cell proliferation, is a histone methyltransferase that specifically monomethylates histone H4 lysine 20 (K20; Nishioka et al, 2002; Couture et al, 2005; Xiao et al, 2005; Oda et al, 2009). To investigate whether the expression patterns of H4K20me1 is associated with the increase of Pr-set7 during NSC reactivation, we examined the H4K20me1 level at 0 h and 24 h ALH. As shown in Fig EV2A–C, at 0 h ALH, the level of H4K20me1 in control brains and NSCs was nearly absent. At this stage, H4K20me1 could only be clearly detected in mitotic NSCs with condensed chromosomes, likely due to the insensitivity of anti-H4K20me1 antibody to the weak signal. By contrast, at 24 h ALH, H4K20me1 levels in both NSCs and brain lobes were increased significantly and its nuclear staining could also be detected in interphase NSCs (Fig EV2A–C). Therefore, the increased H4K20me1 level was associated with the increased Pr-set7 level during NSC reactivation. We then sought to examine whether H4K20me1 was lost in *pr-set7* mutant brains. At 24 h ALH, all mitotic NSCs were H4K20me1-positive (Fig 2C). By contrast, only 11.5% of mitotic NSCs from *pr-set7* mutant contained H4K20me1 (Fig 2C). The remaining H4K20me1 in *pr-set7* mutant might be due to the maternal component, as it was completely lost in the third instar larval stage (Fig EV2D). The loss of H4K20 monomethylation could be well restored upon expression of either UAS-*pr-set7* under *insc-Gal4* (Fig 2C; H4K20me1 in 86.8% mitotic NSCs) or the genomic *pr-set7*-BAC (Fig 2C; H4K20me1 in 95.2% mitotic NSCs). These data suggest that the H4K20 monomethylation is lost in *pr-set7* mutant larval brains.

Pr-set7 is required for the reactivation of both G₀- and G₂-arrested quiescent NSCs

Drosophila quiescent NSCs arrest in either G₀ or G₂ quiescent states (Otsuki & Brand, 2018). To explore which population of quiescent

NSCs requires Pr-set7's function in reactivation, we took the advantage of the fly-FUCCI system, a dual-color fluorescent reporter (UAS-GFP.E2f1.1-230, UAS-mRFP1.CycB.1-266; BDSC#55117) for cell cycle stages (Zielke et al, 2014; Fig 2D). Quiescent NSCs were marked by nuclear Prospero (Pros), as transient Pros expression induces NSC quiescence (Lai & Doe, 2014). G₂ quiescent NSCs were positive for GFP, RFP, and nuclear Pros, while G₀ quiescent NSCs were marked by GFP and nuclear Pros (Fig 2E). At 24 h ALH, the proportion of G₀ and G₂ quiescent NSCs in *pr-set7* mutant closely resembled the distribution in control FUCCI brains (Fig 2F), suggesting that the reactivation of both G₀ and G₂ quiescent NSCs was similarly affected upon loss of *pr-set7*. Therefore, we conclude that Pr-set7 is likely required for the reactivation of both G₀ and G₂ quiescent NSCs.

Pr-set7 binds to *cdk1* and *ebd1* in NSCs in TaDa *in vivo* profiling

To identify the potential targets of Pr-set7 in NSCs during reactivation, we performed targeted DNA adenine methyltransferase (Dam) identification (TaDa). TaDa enables cell type-specific profiling of transcriptome and chromatin binding (Southall et al, 2013). We generated transgenic Dam-Pr-set7 and expressed it or Dam alone (as a control) in NSCs under *grh-Gal4* at 24 h ALH. Samples were subjected to next-generation sequencing (NGS) and bioinformatics analysis (Fig 3A). From two replicates of the DamID analysis, we have identified 7157 binding peaks (with peak score > 50) of Pr-set7 (Dataset EV1). Wnt pathway co-activator *earthbound1* (*ebd1*) was identified among top candidates based on peak scores and *cdk1* was the top candidate among cyclin-dependent kinase (CDKs) and cyclins (Fig 3B, C, Appendix Table S1). Based on TaDa profiling, Pr-set7 binds to the promoter and transcriptional start site of both *ebd1* and *cdk1*, suggesting that Pr-set7 may positively regulate their gene expression in NSCs (Fig 3B and C). GO analysis on DamID data also suggested that these potential targets were enriched for genes regulating various biological processes and nervous system development (Appendix Table S2).

Pr-Set7 is required for the expression of *ebd1* and *cdk1* in the larval brain

To further validate the DamID results that *ebd1* and *cdk1* are bound by Pr-set7, we assessed the mRNA level of *ebd1* and *cdk1* in *pr-set7*

larvae brains. At 24 h ALH, the mRNA levels of *pr-set7* in *pr-set7* mutant brains were decreased to $32.5 \pm 21.2\%$ and $44.8 \pm 22.3\%$ measured by two different pairs of primers, compared with control brains (Fig 3D). This result suggested an efficient depletion of *pr-*

set7 in the mutants. Interestingly, at 24 h ALH, the mRNA level of *cdk1* in *pr-set7* mutant brains was significantly decreased to $64.5 \pm 8.3\%$, compared with the control (Fig 3D). Next, we examined Cdk1 protein levels in whole-brain protein extracts by Western

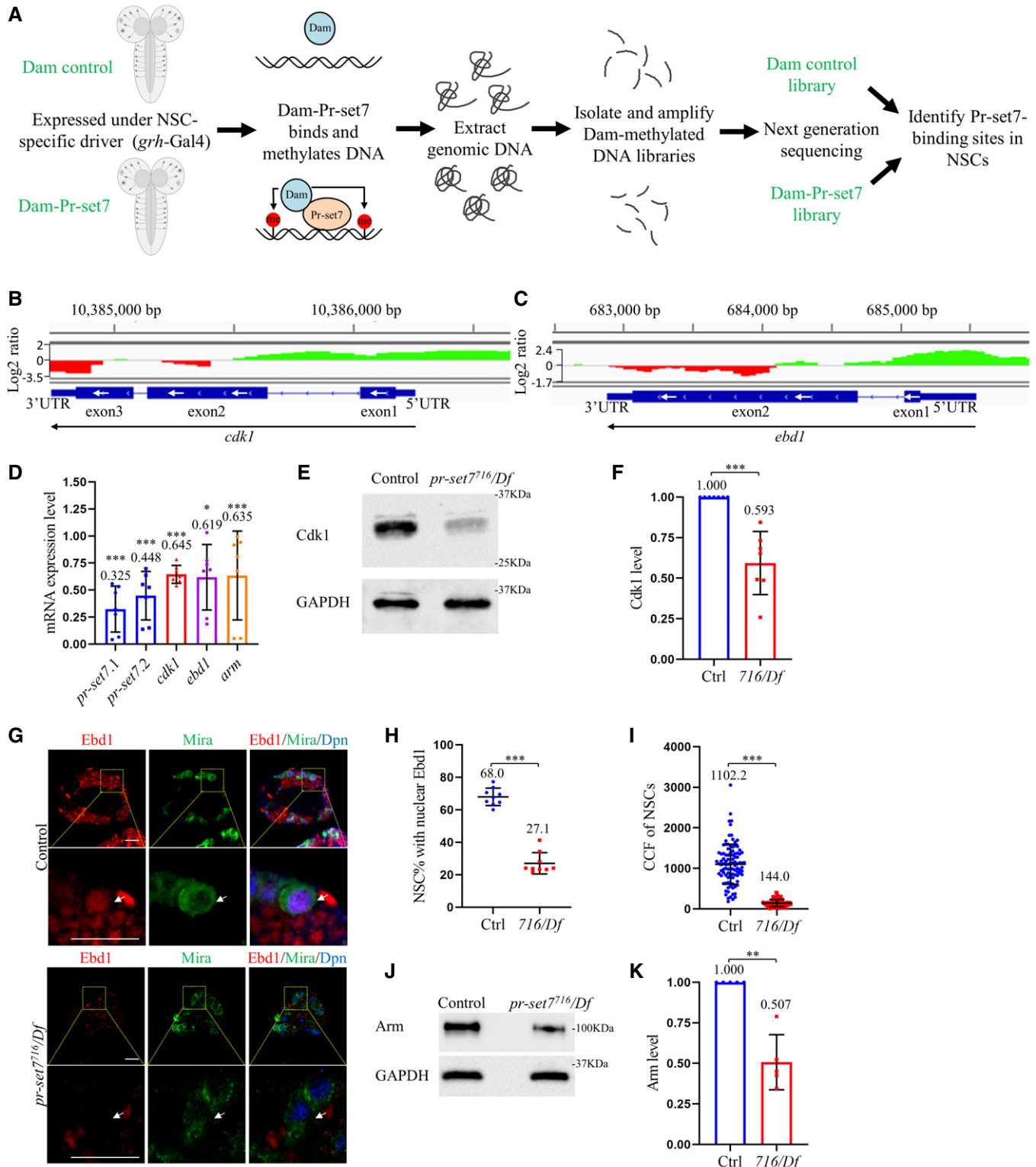


Figure 3.

Figure 3. *cdk1* and *ebd1* are identified as potential targets of Pr-set7 in NSC-specific TaDa in vivo profiling.

- A A schematic representation of the TaDa analysis performed in *Drosophila* NSCs.
- B, C The binding profile of Pr-set7 on *cdk1* gene region (B) and *ebd1* gene region (C) in NSCs. The green peaks represent positive binding and red means no binding, which are based on the log₂ ratio between Dam-Pr-set7 and Dam control (Y-axis).
- D qPCR analysis of *pr-set7*, *cdk1*, *ebd1*, and *arm* in larval brains of control (ctrl; *yw*) and *pr-set7⁷¹⁶/Df(3R)ED5644 (716/Df)* at 24 h ALH. *n* = 7 as biological replicates. Statistical analyses were done comparing between control (GAPDH1, GAPDH2, Tbp1, and Rpl32) and *pr-set7⁷¹⁶/Df*, using Mann–Whitney test. The mRNA levels of control were normalized to 1. Data are presented as mean ± SD calculated from all replicates.
- E Western blot analysis of larval brain extracts of control (ctrl; *yw*) and *pr-set7⁷¹⁶/Df* at 24 h ALH. Blots were probed with anti-Cdk1 antibody and anti-GAPDH1 antibody (loading control).
- F Quantification of normalized Cdk1 intensity against GAPDH in (E). *n* = 7 as biological replicates.
- G Larval NSCs of control (ctrl; *yw*) and *pr-set7⁷¹⁶/Df* at 24 h ALH were stained for Ebd1, Dpn, and Mira. Yellow dotted boxes, zoomed-in area. White arrows point to NSCs.
- H, I Quantifications of nuclear Ebd1 (H) and the corrected total cell fluorescence (CCF) (I) in genotypes in (G). In (H), *n* = 756, 9 BL for control; *n* = 765, 9 BL for *pr-set7⁷¹⁶/Df*. In (I), CCF = Integrated Density – (Area of selected cell × Mean fluorescence of background readings). CCFs were 1102.2 ± 493.2 (*n* = 99) for control (ctrl; *yw*) and 144.0 ± 88.0 (*n* = 98) for 716/Df.
- J Western blot analysis of larval brain extracts of control (ctrl; *yw*) and *pr-set7⁷¹⁶/Df* at 24 h ALH. Blots were probed with anti-Arm antibody or anti-GAPDH1 antibody (loading control).
- K Quantification of normalized Arm levels against GAPDH in (J). *n* = 5 as biological replicates.

Data information: Data are presented in (D, F, H, I, K) as mean ± SD. *n* numbers in (H) were total NSCs counted with total brain lobes measured, while each brain lobe was considered as one biological replicate. Statistical analyses were done comparing two different genotypes using Mann–Whitney test (D, F, H, I, K). **P* < 0.05, ***P* < 0.01, and ****P* < 0.001. Scale bars, 15 μm (G). Source data are available online for this figure.

blot. Remarkably, Cdk1 protein levels were decreased significantly to 59.3 ± 19.5% in *pr-set7* mutant larval brains, compared with the control brains at 24 h ALH (Fig 3E and F). Taken together, Pr-set7 binds to *cdk1* promoter region and promotes its expression in NSCs.

Similarly, at 24 h ALH, the mRNA level of *ebd1* in the *pr-set7* mutant was significantly decreased to 61.9 ± 30.3% of the control (Fig 3D). At 24 h ALH, Ebd1 protein was detected in the nucleus of control NSCs during interphase (Fig 3G–I; 68.0 ± 5.4%). This is consistent with the nuclear localization of Ebd1 in neurons (Benchabane *et al*, 2011). However, Ebd1 protein in central brains upon *pr-set7* depletion was nearly absent at 24 h ALH, with only 27.1 ± 6.6% of them showed weak nuclear Ebd1 (Fig 3G–I). Ebd1 promotes interaction between the Wnt/Wingless pathway co-activators β-catenin/Armadillo (Arm) and T-cell factor (TCF) and recruitment of β-catenin to chromatin (Benchabane *et al*, 2011). Interestingly, in the *pr-set7* mutant, mRNA of *arm* was reduced to 63.5 ± 44.1% of control at 24 h ALH in the whole larval brain (Fig 3D). Similarly, the protein level of Arm was also significantly decreased to 50.7 ± 17.0% of control at 24 h ALH in whole larval brain extracts (Fig 3J and K). These observations suggest that Pr-set7 may promote Ebd1 expression to activate Wnt/Wingless signaling.

As H4K20me1 correlates with both gene expression and repression, we wondered whether Pr-set7 could both promote and repress gene expression. We surveyed a few genes including *cyclin E* (*cycE*), *pangolin* (*pan*), *frizzled 2* (*fz2*), and *pyridoxal kinase* (*pdck*), and examined the changes of their transcript level in the *pr-set7* mutant brain by qPCR. *CycE* is not a target of Pr-set7 in DamID and was selected as it is a cell-cycle gene. *Pan* and *Fz2* are Wnt signaling components (Brunner *et al*, 1997; Swarup & Verheyen, 2012). *Pan* is identified as a potential target of Pr-set7 in DamID in this study (Appendix Table S1), while *fz2* is not. The *Pan* mammalian homology, *Lef-1/Tcf7* is upregulated by Pr-set7 in mammalian cells (Li *et al*, 2011). *Pyridoxal kinase* (*pdck*) was identified as potential Pr-set7 targets in *Drosophila* in our DamID analysis (Appendix Table S1), while mammalian *pdck* is downregulated by Pr-set7 in mammalian systems (Congdon *et al*, 2010). We found that in *pr-set7* mutant brains at 24 h ALH, the mRNA levels of *cycE* and *pan* were downregulated, while *pdck* was upregulated, compared to the control (Fig EV2E). The mRNA level of *fz2* and

cyclinJ (*cycJ*), which were not targets of Pr-set7 in DamID, had no significant change in *pr-set7* mutant brains (Fig EV2E). Therefore, Pr-set7 could activate and repress different genes and should not be considered as a sole activator or repressor.

Cdk1 is both necessary and sufficient to promote NSC reactivation on fed condition

Given that Pr-set7 promotes the expression of Cdk1 in NSCs, we investigated the role of Cdk1 during NSC reactivation. At 24 h ALH at 29°C, control NSCs were mostly reactivated; Only 5.2 ± 1.7% of them showed cellular process (Fig 4A and B) and 10.5 ± 3.3% of NSCs lacked EdU incorporation (Fig 4C and D). By contrast, in *cdk1* RNAi knockdown (BDSC#35350) brains at the same condition, 17.5 ± 2.9% of NSCs showed cellular processes (Fig 4A and B) and 93.5 ± 2.1% of NSCs failed to incorporate EdU (Fig 4C and D). Two other *cdk1* RNAi lines (BDSC#36117 and BDSC#40950) showed similar defects of NSC reactivation, as indicated by the significant increase in the number of NSCs retaining cellular extension, concomitant with a dramatic decrease of the number of EdU-positive NSCs (Fig 4C and D). Next, we examined *cdk1^{B47}*, an amorphic allele that contains a point mutation at the splice donor site of 5' end of first intron (Clegg *et al*, 1993). In control brains at 24 h ALH, most NSCs are reactivated with only 6.4 ± 1.6% showed cellular process (Fig EV3A and B). In comparison, 16.6 ± 2.7% of *cdk1^{B47}* mutant NSC exhibited cellular extension (Fig EV3A and B). Remarkably, 91.2 ± 2.2% of *cdk1^{B47}* mutant NSCs failed to incorporate EdU, compared with 13.9 ± 4.4% of control NSCs (Fig EV3C and D). These observations indicate that Cdk1 is intrinsically required for NSC reactivation.

To test whether Cdk1 overexpression is sufficient to trigger NSC reactivation, we overexpressed *cdk1*-Myc in NSCs under the control of *insc*-Gal4. At 6 h ALH, most control NSCs remained in quiescence and only 22.5 ± 7.2% of NSCs incorporated EdU (Fig 4E and F). NSC diameter was 4.5 ± 0.8 μm at this stage (Fig 4G). By contrast, 63.3 ± 4.1% of NSCs incorporated EdU upon *cdk1* overexpression (Fig 4E and F) and NSC diameter was increased significantly to 5.4 ± 0.7 μm (Fig 4G). Cdk1 is negatively regulated by Wee1 and Myt1 via phosphorylation on residues T14 and Y15 (Ayeni *et al*,

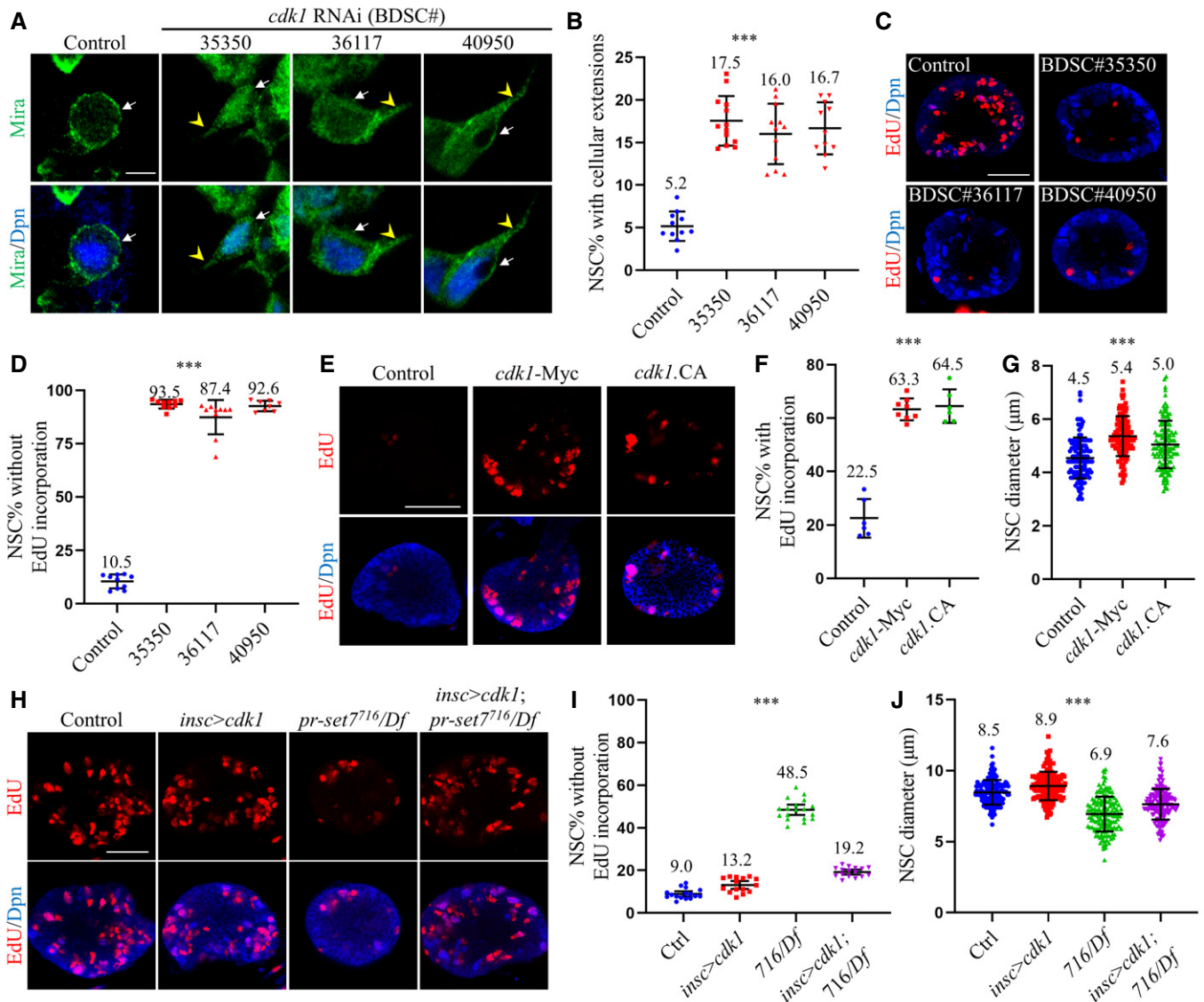


Figure 4. Cdk1 functions downstream of Pr-set7 and is both necessary and sufficient for NSC reactivation on fed condition.

A Larval brains of control and *cdk1* RNAi (BDSC#35350, #36117, and #40950) under *insc*-Gal4 at 24 h ALH were stained for Deadpan (Dpn) and Miranda (Mira).
 B Quantifications of cellular extensions for genotypes in (A). Control: $n = 942$, 11 BL; BDSC#35350: $n = 1056$, 13 BL; BDSC#36117: $16.0 \pm 3.5\%$ ($n = 1059$, 12 BL); BDSC#40950: $16.7 \pm 3.1\%$ ($n = 933$, 11 BL).
 C Larval brains of control and *cdk1* RNAi (BDSC#35350, #36117, and #40950) under *insc*-Gal4 at 24 h ALH were labeled with Dpn and EdU.
 D Quantifications of NSCs without EdU incorporation for genotypes in (C). Control: $n = 849$, 10 BL; BDSC#35350: $n = 741$, 10 BL; BDSC#36117: $87.4 \pm 8.0\%$ ($n = 697$, 10 BL); BDSC#40950: $92.6 \pm 2.4\%$ ($n = 621$, 8 BL).
 E Larval brains of control, UAS-*cdk1*-Myc, and UAS-*cdk1*.T14A.Y15F.VFP (*cdk1*.CA) under *insc*-Gal4 at 6 h ALH were labeled with Dpn and EdU.
 F, G Quantifications of EdU incorporation (F) and NSC diameters (G) for genotypes in (E). In (F), $n = 345$, 6 BL for control; $n = 524$, 8 BL for *cdk1*-Myc and $n = 280$, 6 BL for *cdk1*.CA. In (G), $n = 123$ for control; $n = 135$ for *cdk1*-Myc and $n = 137$ for *cdk1*.CA.
 H Larval brains of control (ctrl; *yw*), *cdk1*-Myc overexpression under *insc*-Gal4, *pr-set7*^{7/16}/Df (*pr-set7*^{7/16}/Df; *ED5644* (716/Df)), and *pr-set7*^{7/16}/Df with *cdk1*-Myc induced with *insc*-Gal4 at 24 h ALH were labeled with Dpn and EdU.
 I, J Quantifications of EdU incorporation (I) and NSC diameters (J) for genotypes in (H). In (I), $n = 1334$, 16 BL for control; $n = 1299$, 15 BL for *insc > cdk1*; $n = 1221$, 18 BL for *pr-set7*^{7/16}/Df and $n = 1372$, 16 BL for *pr-set7*^{7/16}/Df with *cdk1*-Myc induced with *insc*-Gal4. In (J), $n = 153$ for control; $n = 152$ for *insc > cdk1*; $n = 156$ for *pr-set7*^{7/16}/Df and $n = 159$ for *pr-set7*^{7/16}/Df with *cdk1*-Myc induced with *insc*-Gal4.

Data information: Data were presented in quantification graphs as mean \pm SD (B, D, F, G, I, J). n numbers in (B, D, F, I) were total NSCs counted with total brain lobes measured, while each brain lobe was considered as one biological replicate. White arrows point to NSCs and yellow arrowheads point to cellular extensions of NSCs (A). Statistical analyses were done comparing among different genotypes using ordinary one-way ANOVA (B, D, F, G, I, J). $***P < 0.001$. Scale bars, 5 μ m (A), 30 μ m (C, E, H). Control: *insc*-Gal4/+ UAS-*dicer2* in (A–G).

2014). Upon overexpression of Cdk1.T14A.Y15F, an active form of Cdk1 that is unable to be phosphorylated by Wee1 and Myt1, under *insc-Gal4*, $64.5 \pm 6.3\%$ of NSCs (Fig 4E and F) incorporated EdU and the NSC diameter was increased to $5.0 \pm 0.9 \mu\text{m}$ (Fig 4G). These results suggest that Cdk1 overexpression leads to premature NSC reactivation. However, in the absence of dietary amino acids (sucrose-only food), Cdk1 overexpression did not have any effect on reactivation (Fig EV3E and F). Taken together, Cdk1 is both necessary and sufficient for NSC reactivation in the presence of dietary amino acids.

Cdk1 overexpression significantly suppresses NSC reactivation defects observed in *pr-set7* mutants

We investigated whether Cdk1 overexpression could suppress NSC quiescence phenotype in *pr-set7* mutant brains. At 24 h ALH, most of control NSCs were reactivated (Fig 4H and I; $9.0 \pm 2.4\%$ NSCs without EdU incorporation; Fig EV3G and H; $7.3 \pm 2.3\%$ NSCs retain cellular extensions). At 24 h ALH, Cdk1-Myc overexpression behaved similarly to control with only $13.2 \pm 3.4\%$ EdU-negative NSCs (Fig 4H and I) and $6.9 \pm 1.6\%$ retaining cellular extensions (Fig EV3G and H). In *pr-set7* mutant brains, $48.5 \pm 4.8\%$ NSCs failed to incorporate EdU (Fig 4H and I) and $20.7 \pm 2.0\%$ NSCs retained cellular extensions (Fig EV3G and H). By contrast, in *pr-set7* NSCs with Cdk1 overexpression, only $19.2 \pm 2.3\%$ of NSCs did not incorporate EdU (Fig 4H and I) and the percentage of NSCs with cellular extensions was decreased to $11.1 \pm 1.8\%$ (Fig EV3G and H). The cell growth defect of *pr-set7* NSCs was also partially suppressed by Cdk1 overexpression, as the diameter was increased to $7.6 \pm 1.1 \mu\text{m}$ (Fig 4J), which is significantly greater than $6.9 \pm 1.2 \mu\text{m}$ (Fig 4J) in the *pr-set7* mutant, but smaller than $8.5 \pm 0.9 \mu\text{m}$ (Fig 4J) and $8.9 \pm 1.0 \mu\text{m}$ (Fig 4J) in control or Cdk1 overexpression alone. This significant suppression strongly supports our conclusion that Pr-set7 promotes NSC reactivation primarily through upregulating Cdk1 expression.

Wingless pathway transcriptional co-activator Ebd1 is required for NSC reactivation

Next, we sought to investigate the function of Ebd1 during NSC reactivation. *ebd1²⁴⁰* is a loss-of-function allele containing a 2,925

base pair (bp) deletion by a P-element imprecise excision that removes the N-terminal (308–3232 bp) part of the gene (Benchaane *et al*, 2011). At 24 h ALH, most control NSCs were reactivated, with only $6.9 \pm 2.4\%$ of them showed cellular extension (Fig 5A and B). In comparison, $15.9 \pm 1.8\%$ of *ebd1²⁴⁰* NSCs displayed cellular extension (Fig 5A and B). Consistent with this observation, $12.3 \pm 3.4\%$ of control NSCs lacked EdU incorporation at 24 h ALH (Fig 5C and D), while $56.9 \pm 3.8\%$ of *ebd1²⁴⁰* NSCs failed to incorporate EdU (Fig 5C and D). The function of Ebd1 in NSC reactivation was confirmed using *ebd1* RNAi knockdown (BDSC#35765) under the *insc-Gal4* driver (Fig EV4A and D). Taken together, these observations indicate that Wnt signaling co-activator Ebd1 promotes *Drosophila* NSC reactivation.

In order to investigate whether Ebd1 in the NSC is only required for NSC reactivation or maintenance of NSC proliferation status, we performed a time-course analysis of *ebd1²⁴⁰* mutant and examined cellular protrusion of quiescent NSCs. At 48 h ALH, almost all control NSCs were reactivated, with only $0.2 \pm 0.5\%$ of them still showed cellular extensions (Fig EV5C). Similarly, only $2.2 \pm 0.9\%$ of *ebd1²⁴⁰* NSCs still retained cellular extensions at the same time (Fig EV5C). At later time points (72 h and 96 h ALH), all control and *ebd1²⁴⁰* NSCs lost their cellular extensions (Fig EV5C). These data suggest that Ebd1 is important for NSC reactivation, but not for preventing NSCs from re-entering into quiescence at later larval stages. We next examined the EdU incorporation in a time-course study. At 24 h ALH, only $13.0 \pm 2.2\%$ (Fig EV5A and B) of control NSCs lacked EdU incorporation. By contrast, $69.4 \pm 7.2\%$ (Fig EV5A and B) of *ebd1²⁴⁰* NSCs failed to incorporate EdU at the same time. This observation suggests that NSC reactivation is defective in *ebd1²⁴⁰* at early larval stages. At 48 h ALH, most of the control NSCs were reactivated, with only $1.4 \pm 1.3\%$ (Fig EV5A and B) of them failed to incorporate EdU. In comparison, for *ebd1²⁴⁰* NSCs, $34.6 \pm 3.0\%$ of them still failed to incorporate EdU. At later time points, all control NSCs were reactivated with EdU incorporation at 72 h ALH and 96 h ALH (Fig EV5A and B). In contrast, in *ebd1²⁴⁰* brains, $27.6 \pm 5.0\%$ at 72 h ALH and $27.4 \pm 3.9\%$ at 96 h ALH of NSCs failed to incorporate EdU (Fig EV5A and B). These observations suggested that NSCs in the *ebd1* mutant were not fully reactivated. Moreover, *ebd1* overexpression under *insc-Gal4* at 6 h ALH

Figure 5. Ebd1 promotes NSC reactivation and its overexpression suppresses NSC reactivation defects in *pr-set7* mutants.

- A Larval NSCs of control (ctrl; *yw*) and *ebd1²⁴⁰* at 24 h ALH were stained for Deadpan (Dpn) and Miranda (Mira).
 B Quantifications of cellular extensions for genotypes in (A). Control: $n = 886$, 11 BL; *ebd1²⁴⁰*: $n = 864$, 12 BL.
 C Larval brains of control (ctrl; *yw*) and *ebd1²⁴⁰* at 24 h ALH were labeled with Dpn and EdU.
 D Quantifications of NSC without EdU incorporation for genotypes in (C). Control: $n = 1034$, 12 BL; *ebd1²⁴⁰*: $n = 1139$, 16 BL.
 E Larval NSCs of *grainyhead* (*grh*) > CD8-GFP at 0, 24, and 48 h ALH were stained for CD8, Dpn, and Ebd1. Yellow dotted boxes indicate the region of zoomed-in images.
 F, G Quantifications of nuclear/cytoplasmic Ebd1 (F) and the corrected total cell fluorescence (CCF) of Ebd1 in NSCs (G) for genotypes in (E). In (F), $n = 1044$, 14 BL at 0 h ALH; $n = 712$, 10 BL at 24 h ALH and $n = 1122$, 11 BL. In (G), CCF = Integrated Density – (area of selected cell × mean fluorescence of background readings). For CCFs of Ebd1, 128.5 ± 140.7 ($n = 162$) at 0 h ALH, 938.7 ± 1176.8 ($n = 150$) at 24 h ALH and 1868.2 ± 1025.1 ($n = 161$) at 48 h ALH.
 H Larval brains of control (ctrl; *yw*), *ebd1*-Flag overexpression under *insc-Gal4*, *pr-set7⁷¹⁶/Df(3R)ED5644* (*716/Df*) and *pr-set7⁷¹⁶/Df* with *ebd1* induced with *insc-Gal4* at 24 h ALH were labeled with Dpn and EdU.
 I Quantifications of NSCs without EdU incorporation for larval brains in (H). Control: $n = 1162$, 13 BL; *insc* > *ebd1*: $n = 997$, 11 BL; *pr-set7⁷¹⁶/Df*: $n = 928$, 13 BL and *pr-set7⁷¹⁶/Df* with *ebd1* induced with *insc-Gal4*: $n = 1284$, 16 BL.

Data information: Data are presented in (B, D, F, G, I) as mean \pm SD. n numbers in (B, D, F, I) were total NSCs counted with total brain lobes measured, while each brain lobe was considered as one biological replicate. White arrows point to NSCs and yellow arrowheads point to cellular extensions of NSCs (A, E). Statistical analyses were done comparing two different genotypes using Mann–Whitney test (B, D, F). For F, statistical analyses were done comparing the percentage at later time points with the ones at 0 h ALH. Statistical analyses were done comparing among different genotypes using ordinary one-way ANOVA (G, I). ns: non-significant; * $P < 0.05$; *** $P < 0.001$. Scale bars, 5 μm (A), 15 μm (E), 30 μm (C, H).

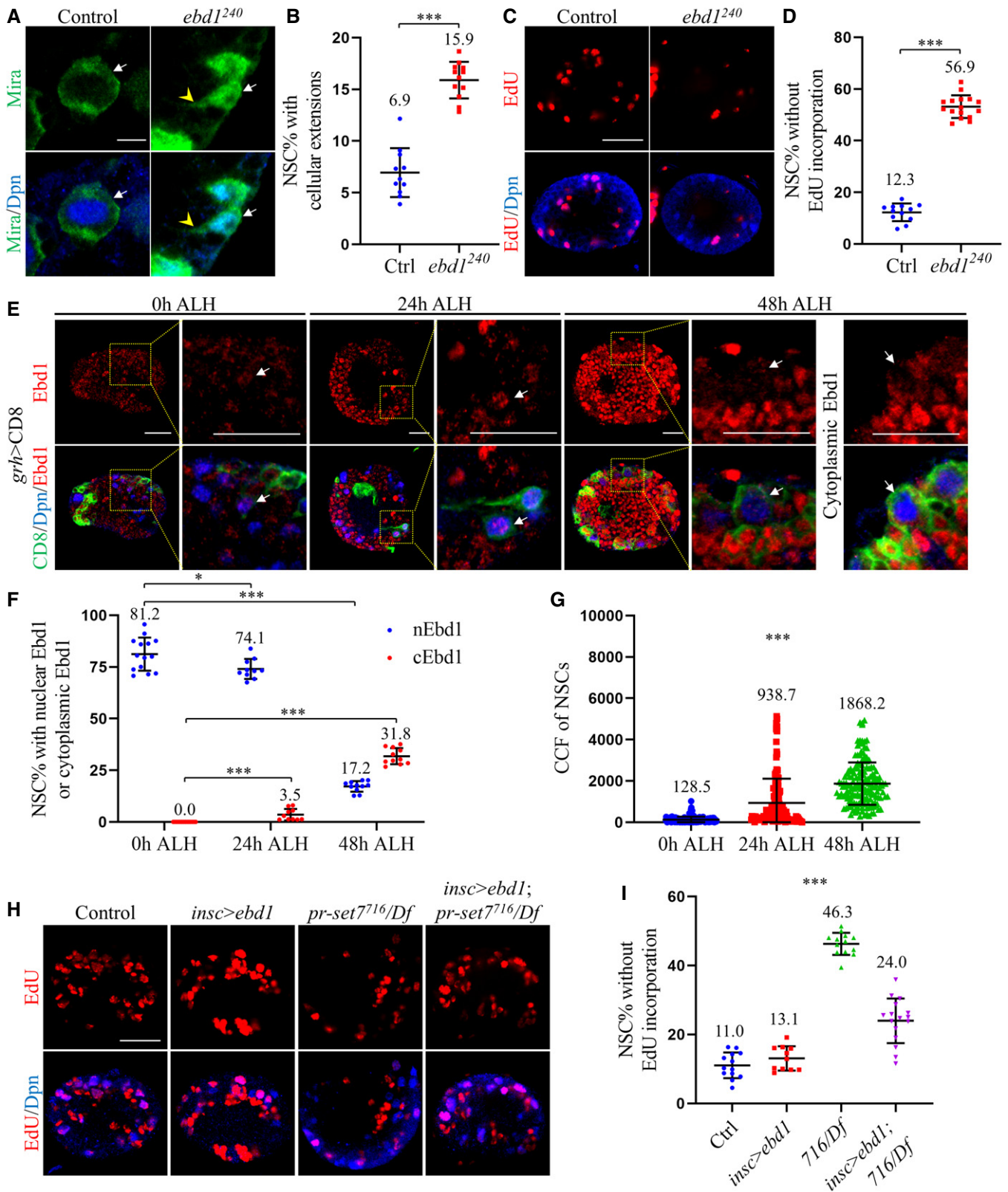


Figure 5.

at 29°C was insufficient to trigger precocious cell cycle re-entry (Fig EV5D and E).

Ebd1 is transiently localized to the nucleus of quiescent and reactivating NSCs

As Ebd1 is required for NSC reactivation, we sought to examine the level of Ebd1 in the larval brain in a time-course analysis. Ebd1 was reported to localize in the nucleus of neurons (Benchabane *et al*, 2011), but its localization pattern in NSCs was unknown. Although the overall level of Ebd1 in the brain was low at 0 h and 24 h ALH, Ebd1 was observed primarily in the nucleus of NSCs (Fig 5E and F; $81.2 \pm 8.0\%$ at 0 h ALH; $74.1 \pm 4.9\%$ at 24 h ALH). At 48 h ALH, nuclear Ebd1 was only observed in $17.2 \pm 2.6\%$ of NSCs and was highly expressed in neurons (Fig 5E and F). Concomitantly, cytoplasmic Ebd1 increased over developmental time; it was nearly undetectable in NSCs at 0 h ALH (0%) and 24 h ALH ($3.5 \pm 2.8\%$) and was observed in $31.8 \pm 3.9\%$ of NSCs at 48 h ALH. In contrast to decreased nuclear Ebd1 in NSCs, the overall level of Ebd1 in NSCs still increased from 0 h ALH to 48 h ALH (Fig 5E and G). Our observations suggest that nuclear Ebd1 is transiently detected in the nucleus of quiescent and reactivating NSCs and lost following NSC reactivation.

Ebd1 overexpression significantly suppresses NSC reactivation defects observed upon loss of *pr-set7*

Given that Ebd1 is required for NSC reactivation, we investigated whether Ebd1 overexpression could suppress NSC reactivation defects observed in *pr-set7* mutant brains. At 24 h ALH, vast majority of control NSCs and Flag-Ebd1 overexpressing NSCs were reactivated, with only $11.0 \pm 3.7\%$ and $13.1 \pm 3.5\%$ lacked EdU incorporation (Fig 5H and I). In *pr-set7* mutant, NSC reactivation defects were evident, as $46.3 \pm 3.2\%$ (Fig 5H and I) NSCs failed to incorporate EdU. By contrast, in *pr-set7* NSCs with Ebd1 overexpression, the percentages of EdU-negative NSCs were decreased significantly to $24.0 \pm 6.5\%$ (Fig 5H and I). In addition, at 24 h ALH in *pr-set7* mutant with Ebd1 overexpression, NSCs retaining cellular protrusion was significantly decreased to $13.7 \pm 1.9\%$, compared with $22.0 \pm 2.8\%$ of NSCs in *pr-set7* (Fig EV4F and G). The rescue was partial, as there were only $8.8 \pm 1.3\%$ and $10.3 \pm 1.8\%$ of

NSCs in control and Ebd1 overexpressing brains retaining cellular extensions at the same condition (Fig EV4F and G). Similar to Cdk1 overexpression, Ebd1 overexpression could partially suppress the cell growth defect of *pr-set7* NSCs. The diameter of *pr-set7* mutant NSCs was $6.6 \pm 1.0 \mu\text{m}$ at 24 h ALH (Fig EV4E). In comparison, the diameter of *pr-set7* NSCs with Ebd1 overexpression was significantly increased to $8.2 \pm 1.0 \mu\text{m}$ (Fig EV4E), very close to the size of control (Fig EV4E; $8.5 \pm 0.9 \mu\text{m}$) and Ebd1 overexpression alone (Fig EV4E; $8.7 \pm 1.0 \mu\text{m}$). Taken together, we conclude that Pr-set7 promotes the expression of Wingless pathway transcriptional co-activator Ebd1 to facilitate NSC reactivation.

Reciprocal regulations between Cdk1 and Ebd1 in NSCs

To probe the possible interaction between Ebd1 and Cdk1 during NSC reactivation, we first examined whether Cdk1 regulates Ebd1 in NSCs. When *cdk1^{B47}* was depleted, Ebd1 levels in NSCs, as detected by immunostaining, were significantly decreased, compared with that of control NSCs at 24 h ALH (Fig 6A and B). There were no significant changes in the fluorescence intensity of nuclear Dpn, an internal control, in NSCs between the control and the *cdk1^{B47}* mutant (Fig EV5F). The Ebd1 level in the whole larval brain was also significantly decreased in *cdk1^{B47}* (Fig EV5G), but not as dramatic as the changes of Ebd1 in NSCs. Next, we examined the levels of Ebd1 upon Cdk1 overexpression in NSCs. At 6 h ALH at 29°C, Ebd1 levels, but not nuclear Dpn, were significantly increased in NSCs and whole brains when *cdk1* was overexpressed under *insc-Gal4*, as compared with control at the same condition (Fig 6C and D; Fig EV5H and I). Taken together, these results suggest that Cdk1 upregulates Ebd1 levels in NSCs in early larval stages.

We then investigated whether Ebd1 potentially regulates Cdk1 in NSCs. As anti-Cdk1 antibodies did not work for immunofluorescence in the larval brain, we examined the mRNA level of *cdk1* upon *ebd1* depletion by qPCR. Surprisingly, upon *ebd1* depletion in *ebd1²⁴⁰*, *cdk1* mRNA was upregulated to $250 \pm 30\%$ in *ebd1²⁴⁰* brains (Fig 6E). Therefore, Cdk1 and Ebd1 might regulate each other in a negative feedback loop to maintain an equilibrium of Cdk1 and Ebd1 levels during NSC reactivation.

In order to further investigate how the Wingless/Wnt pathway is affected upon loss of *pr-set7* or *cdk1*, we examined the expression of Senseless (Sens) in *pr-set7* and *cdk1* mutants. Sens is a downstream

Figure 6. A reciprocal regulation between Cdk1 and Ebd1 during NSC reactivation.

- A Larval NSCs of control (ctrl; *yw*) and *cdk1^{B47}* at 24 h ALH were labeled for Earthbound1 (Ebd1), Deadpan (Dpn), and Miranda (Mira).
 B Quantifications of the corrected total cell fluorescence (CCF) of Ebd1 in genotypes in (A). CCF = Integrated Density – (Area of selected cell × Mean fluorescence of background readings). CCFs were 846.9 ± 394.2 for control (ctrl; *yw*; $n = 167$, 14 BL) and 354.3 ± 245.3 for *cdk1^{B47}* ($n = 211$, 13 BL).
 C, D Larval NSCs of control (*UAS-dicer2*) and *UAS-cdk1-Myc* induced with *insc-Gal4* at 6 h ALH were labeled for Ebd1, Dpn, and Mira. (D) Quantifications of the CCF of Ebd1 in genotypes in (C). CCFs were 111.3 ± 80.2 for control ($n = 157$, 12 BL) and 346.6 ± 221.1 for *cdk1-Myc* ($n = 181$, 12 BL).
 E qPCR analysis of *cdk1* in larval brains of control (ctrl; *yw*) and *ebd1²⁴⁰* at 24 h ALH. $n = 3$ as biological replicates. Statistical analyses were done comparing control (GAPDH1, GAPDH2, Tbp1 and Rpl32) and *ebd1²⁴⁰*, using two-tailed Student's *t*-test. The mRNA levels of control were normalized to 1.
 F, G Larval NSCs of control (ctrl; *yw*), *ebd1²⁴⁰* and *pr-set7⁷¹⁶/Df(3R)ED5644 (716/Df)* at 24 h ALH were stained for Senseless (Sens), Dpn, and Mira. (F) Quantifications of the CCF in genotypes in (G). CCFs were 1349.7 ± 792.5 for control ($n = 166$, 13 BL), 505.8 ± 395.9 for *ebd1²⁴⁰* ($n = 206$, 14 BL), and 859.7 ± 619.0 for *716/Df* ($n = 174$, 13 BL).
 H A working model. Pr-Set7 promotes NSC reactivation by positively regulating Cdk1 and Wingless pathway transcriptional co-activator Ebd1 in NSCs. Cdk1 upregulates Ebd1 in NSCs, while Ebd1 may maintain an equilibrium of Cdk1 level during reactivation.

Data information: Data are presented in (B, D, E, G) as mean \pm SD. n numbers in (B, D, G) were total NSCs counted with total brain lobes measured, while each NSC was considered as one biological replicate. White arrows point to NSCs (A, C, F). Yellow dotted boxes indicate the region of zoomed-in images (A, C, F). Statistical analyses were done comparing between two different genotypes using Mann–Whitney test (B, D) and two-tailed Student's *t*-test (E). Statistical analyses were done comparing among different genotypes using ordinary one-way ANOVA (G). * $P < 0.05$; *** $P < 0.001$. Scale bars, 15 μm (A, C, F).

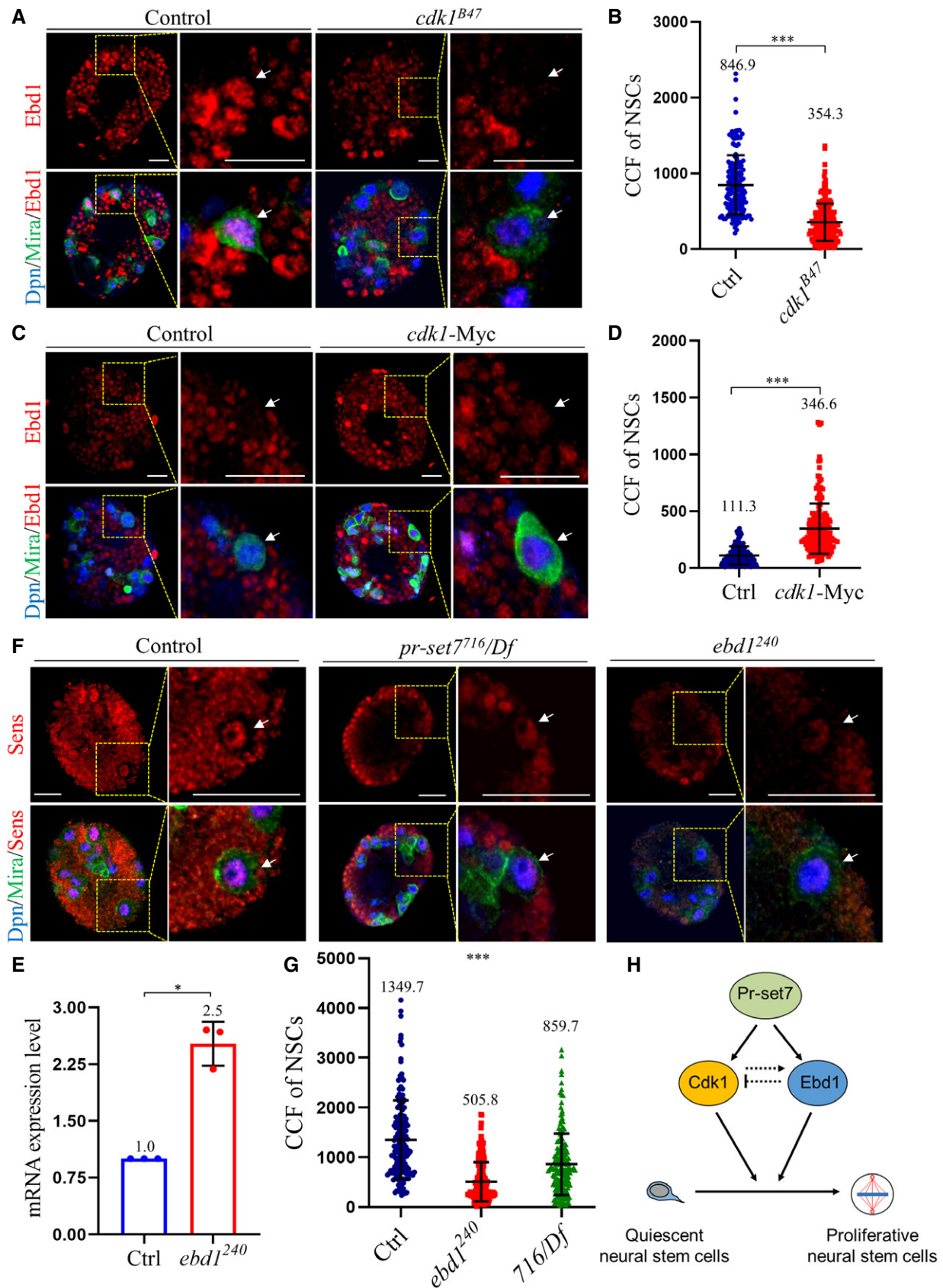


Figure 6.

target of the wingless/Wnt pathway (Baig-Lewis *et al*, 2007; Swarup & Verheyen, 2012), and therefore, it was used as an indicator of Wnt pathway activity. At 24 h ALH, the levels of Sens in NSCs of *ebd1*²⁴⁰ (Fig 6F and G) and *pr-set7*⁷¹⁶/*Df* (Fig 6F and G) were significantly lower than that of control NSCs. This further indicates that loss of *pr-set7* or *ebd1* impairs Wnt pathway activation (Fig 6H).

Discussion

Here, we show that H4K20 monomethyltransferase Pr-set7/SET8 is required for the reactivation of *Drosophila* NSCs. Mechanistically, Pr-set7 promotes the transcription of cell-cycle regulator *cdk1* and Wnt pathway transcriptional co-activator *ebd1*, likely via direct binding to their promoter region. Both Cdk1 and Ebd1 are intrinsically required for NSC reactivation and their overexpression significantly suppresses defects of reactivation observed in *pr-set7* mutant NSCs. Therefore, we demonstrate that Pr-set7, the sole histone H4 K20 methyltransferase, promotes NSC reactivation through regulating Wnt signaling and cell-cycle progression.

Unlike a well-established role for di- and tri-methylation of H4K20 (H4K20me2/3) in gene repression (Schotta *et al*, 2004; Fodor *et al*, 2010), the role of Pr-set7 and H4K20me1 in transcriptional regulation remains highly controversial. H4K20me1 caused chromatin condensation, suggesting that it is a repressor mark (Lu *et al*, 2008; Oda *et al*, 2009). In mammalian cells, H4K20me1 also recruits L3MBTL1, an H4K20me1 and H4K20me2 reader involved in compacting nucleosomes (Trojer *et al*, 2007). In support of this notion, *Drosophila* H4K20me1 was found exclusively in regions without active transcription in Polytene chromosomes (Nishioka *et al*, 2002) and mouse H4K20me1 was enriched on the inactive X chromosome (Kohlmaier *et al*, 2004). Furthermore, in HeLa cells, loss of *pr-set7* led to upregulation of H4K20me1-enriched genes (Congdon *et al*, 2010). However, the genome-wide analysis provided evidence for the role of H4K20me1 in transcriptional activation (Barski *et al*, 2007; Wang *et al*, 2008; Cui *et al*, 2009). In certain genomic loci of mammalian cells including murine erythroleukemia cells, adipocytes, and HeLa cells, H4K20me1 correlated with gene activation (Talasza *et al*, 2005; Vakoc *et al*, 2006; Wakabayashi *et al*, 2009). In our Tada profiling, we demonstrate that Pr-set7 binds to the promoter and transcriptional start site of *cdk1* and *ebd1* and loss of *pr-set7* led to downregulation of *cdk1* and *ebd1* in NSCs. This result is in line with previous reports that Pr-set7 is linked to gene activation (Barski *et al*, 2007; Wang *et al*, 2008; Cui *et al*, 2009). We also show that Pr-set7 could potentially activate and repress different genes in NSCs and should not be considered as a sole activator or repressor. The function of Pr-set7/H4K20me1 may be loci- and cell type-dependent, as Pr-set7 binds to different regions of genes, including promoters, introns, exons, 3'UTRs, and 5'UTRs in our TaDa analysis. Besides functioning as Histone H4 methyl transferase, Pr-set7 also methylates non-histone protein such as PCNA (Takawa *et al*, 2012) and P53 (Shi *et al*, 2007).

We have identified *cdk1* as a major target of Pr-set7 during NSC reactivation through TaDa *in vivo* profiling. We further show that *cdk1* is required for NSC reactivation and is downregulated in the larval brain upon loss of *pr-set7*. Unfortunately, we were unable to determine whether monomethylation of H4K20 occurs at the promoter region of *cdk1* due to technical issues, as the anti-

H4K20me1 antibody did not work in immunoprecipitation in our experiments. Pr-set7 might have additional roles in NSC proliferation at a later larval stage and/or preventing NSCs from re-entering into quiescence because EdU incorporation defects were still observed at later time points between 48 h and 96 h ALH in *pr-set7* mutants, although not as prominent as at 24 h ALH. In addition, cellular protrusions in quiescent NSCs were still retained at 96 h ALH in *pr-set7* mutants, suggesting that *pr-set7* mutants might have failed to re-enter into the cell cycle at later larval stages. However, this defect is unlikely due to slow proliferating NSCs that have re-entered into the cell cycle, because proliferating NSCs would have lost cellular protrusions. Given that Cdk1 has an essential role in the cell cycle regulation and its mutants showed a severe phenotype in NSC reactivation, Cdk1 is likely to be involved in all the above aspects of NSC cell-cycle re-entry.

Our FUCCI analysis showed that the reactivation of both G₂ and G₀ quiescent NSCs were impaired upon loss of *pr-set7*, likely due to downregulation of *cdk1* expression in these NSCs. In *Drosophila*, G₂-M phase transition is governed by Cdk1 phosphorylation and mitotic Cyclin B (Lee *et al*, 2001; Lee & Orr-Weaver, 2003). In G₂ quiescent NSCs, Tribbles targets Cdc25^{String} for degradation and maintains the inhibition of Cdk1 (Otsuki & Brand, 2018). Our finding is also consistent with previous reports that Cdk1/Cyclin A promotes the G₁-S transition of larval imaginal eye disc cells (Foley *et al*, 1999; Foley & Sprenger, 2001). Pr-set7 has been shown to be phosphorylated by CycB/Cdk1 complex at Ser 29 (S29) residue in human HeLa cells during early mitosis, which results in the removal of Pr-Set7 from mitotic chromosome without affecting its methyltransferase activity (Wu *et al*, 2010). Interestingly, the CDK phosphorylation consensus sequence is conserved in *Drosophila* (Brustel *et al*, 2011). It is conceivable that Pr-set7 promotes the expression of Cdk1 to facilitate the NSC reactivation and cell cycle re-entry, while subsequently Pr-Set7 may be regulated by Cdk1 during mitosis for cell cycle progression.

We have identified Ebd1 as another important target of Pr-set7 contributing to NSC reactivation. Ebd1 is a Wnt/Wingless signaling pathway transcriptional co-activator, and it stabilizes the Arm-TCF complex and facilitates the recruitment of the complex to chromatin (Benchabane *et al*, 2011). We found that the Wingless pathway promotes NSC reactivation (Q. Deng, Y.S. Tan, & H. Wang, unpublished data). In this study, our analysis of Ebd1 suggests that activation of the Wingless pathway is required for NSC reactivation. We observed Ebd1 localizes in the nucleus of quiescent and reactivating NSCs. By contrast, nuclear Ebd1 is absent in NSCs at third instar larvae (Benchabane *et al*, 2011). This observation suggests that Ebd1 expression is developmentally regulated and the Wingless signaling pathway may be transiently activated at the early larval stage during NSC reactivation. We further showed that Pr-set7 promotes Ebd1 expression to activate Wnt/Wingless signaling, as the expression of Arm/ β -catenin in NSCs in the early larval stage is also dependent on Pr-set7. In *Drosophila* wing imaginal discs, Pr-set7 was also shown to bind to Pan/TCF via a direct protein-protein interaction and stabilizes this interaction (Yu *et al*, 2019). In vertebrates, Pr-set7 monomethylates H4K20 at the TCF-binding elements, thereby promoting the transcription of Wnt-activated genes (Brustel *et al*, 2011). Interestingly, in the Juvenile Rat Hippocampus, Pr-set7/H4K20me1 promotes Wnt pathway-related gene expression and ensures proper neurodevelopment (Ke *et al*, 2014). These

studies highlight the importance of the regulation of the Wnt/Wingless pathway by Pr-Set7 during neural development.

Interestingly, we observed a potential reciprocal regulation between Ebd1 and Cdk1 during NSC reactivation. Ebd1 expression at the early larval stage may depend on Cdk1. There are emerging links between cell cycle regulators and Wnt signaling in both *Drosophila* and mammals (Davidson & Niehrs, 2010; Kim et al, 2013; Bryja et al, 2017; Chen et al, 2018). For example, in HeLa cells, Cdk1 phosphorylates B-cell CLL/lymphoma 9 (BCL9) to promote mitotic Wnt signaling (Chen et al, 2018). In *C. elegans*, Cdk1 promotes the release of cortical β -catenin to facilitate spindle rotation (Kim et al, 2013). Our results suggest that Cdk1 may activate Wnt signaling via upregulating Ebd1 during NSC reactivation.

Recent studies have identified multiple variants in KMT5A in patients who suffer from neurodevelopmental disorders or cancer, including seventeen copy number variation and one missense mutation (Wickramasekara & Stessman, 2019). The expression of KMT5A in the mammalian brain is currently poorly understood. Interestingly, in situ hybridization data from the Allen Mouse Brain Atlas showed that *Kmt5a* is expressed in the young adult mouse brain. Moreover, the Allen BrainSpan Atlas showed that human KMT5A is expressed in both embryonic and postnatal brains in various brain regions including the hippocampus and prefrontal cortex (Wickramasekara & Stessman, 2019). Our study on Pr-set7 provides the first in-depth study on the function of Pr-set7 during *Drosophila* brain development. As the association of NSC reactivation defects with neurodevelopment disorders starts to emerge (Ding et al, 2020), future studies are warranted to understand the potential role of mammalian KMT5A/PR-SET7/SETD8 in NSC proliferation and associated neurodevelopmental disorders.

Materials and Methods

Fly stocks and genetics

The fly strains used in this study were *pr-set7*⁷¹⁶, UAS-*pr-set7*, *pr-set7* BAC, UAS-Dam-Pr-set7, and UAS-Dam. *ebd1*²⁴⁰ and UAS-*ebd1*-Flag were kindly provided by Dr Y Ahmed. The following stocks were obtained from Bloomington *Drosophila* Stock Center (BDSC): *Df(3R)ED5644* (BDSC#9090), *pr-set7*^{EY04668} (BDSC#15761), *pr-set7*^{M108086} (BDSC#44742), FUCCI construct (BDSC#55117), *cdk1* RNAi (BDSC#35350, #36117 and #40950), UAS-*cdk1*-Myc (BDSC#6642), UASp-*cdk1*.T14A.Y15F.VFP (BDSC# 65394), *ebd1* RNAi (BDSC#35765), and *cdk1*^{B47} (BDSC#6643). *pr-set7* RNAi (NIG #3307R-3) was obtained from the National Institute of Genetics (NIG).

All experiments with mutants were carried out at 25°C. For RNAi knockdown or overexpression, *Drosophila* larvae were shifted from 25°C to 29°C after larval hatching (ALH) to increase the efficiency. As *pr-set7*^{716/+} heterozygous displayed no NSC reactivation defects between 24 h and 96 h ALH and is indistinguishable from the *yw* control, we have used *yw* as a control for various mutants in this study.

Immunocytochemistry

Larvae were dissected in phosphate-buffered saline (PBS), and larval brains were fixed for 22 min in 0.3% PBS-Triton (PBT) with 4% EM

grade formaldehyde (methanol-free). After three times washing with 0.3% PBT (10 min each), brain samples were blocked with 3% bovine serum albumin (BSA) in 0.3% PBT for 45 min. Blocked brain samples were incubated with primary antibody diluted in 3% BSA overnight at 4°C. Following two times washing with 0.3% PBT (10 min each), brain samples were incubated with secondary antibodies diluted in 0.3% PBT for 90 min. DNA was labeled by ToPro-3 (1:5,000, Invitrogen, Cat#: T3605) or DAPI (1:1,500, Molecular Probes, Cat#: D1306). After two more washing with 0.3% PBT (10 min each), larval brains were mounted in Vector shield (Vector Laboratory) for Confocal microscopy. Confocal images were taken by a Zeiss LSM710 Confocal microscope and processed with Adobe Photoshop CS6 for brightness and contrast adjustment.

Primary antibodies used were as follows: guinea pig anti-Dpn (1:1,000, J Skeath), rat anti-CD8 (1:250, Invitrogen, Cat#: MCD0800), rabbit anti-GFP (1:500, Molecular Probes, Cat#: A21311), mouse anti-Mira (1:40, F. Matsuzaki), rabbit anti-Pr-set7 (1:100; generated in this experiment), Rabbit anti-H4K20me1 (1:50; Millipore, Cat#: 04-735), and guinea pig anti-Ebd1 (1:5,000, Y Ahmed).

EdU pulse-chase analysis

Click-iT[®] EdU Alexa Fluor[®] 555 *Imaging Kit* (Invitrogen) were used in this experiment. Larvae were fed with standard food supplemented with 0.2 mM (2%) EdU for 4 h before dissection. Then, the dissected larval brains were fixed with 4% EM grade formaldehyde in 0.3% PBT for 22 min, followed by three times washing with 0.3% PBT (10 min each). After washing, EdU was detected by Alexa Fluor azide according to the *Click-iT* EdU protocol (Invitrogen). Samples were washed two more times with 0.3% PBT (10 min each) and blocked with 3% BSA for 45 min. Following blocking, larval brains were processed by immunohistochemistry.

Nutritional deprivation of larvae

Within 2 h after larval hatching, larvae were transferred to 5% sucrose and 1% Agar in PBS. Larvae were kept at an appropriate temperature for further analysis.

Quantification of cellular extensions and EdU incorporation

Processed *Drosophila* larval brains were placed with the dorsal side up on confocal slides. The confocal z-stacks were taken from the dorsal surface to the deep layers of the larval brains with 3- μ m intervals (24–30 slides per z-stack). Quantification was carried out using Zen software. The numbers of NSCs with phenotypes such as EdU incorporation and cellular extensions of each brain lobe were counted, and the percentage of each brain lobe was calculated. Each brain lobe was considered as one biological replicate. The final data were shown as mean \pm SD calculated from all brain lobes. Total numbers of NSCs counted were also included as n numbers. For example, “n = 1055, 12 brain lobes [BL]” indicates a total of 1,055 NSCs in 12 brain lobes were counted. NSCs without EdU incorporation was quantified at various time points for NSC quiescence blockage/delay phenotype, while NSCs with EdU incorporation at 6 h ALH were quantified to score precocious NSC reactivation phenotype. Minimum six brain lobes were quantified for each sample in this study.

Quantification of the fluorescence intensity and NSC diameters

Images taken by Zeiss LSM710 Confocal microscope were analyzed, and the fluorescence intensity and NSC diameters were measured by ImageJ. Quantifications were performed using the polygon or free hand selection tool in ImageJ to outline NSCs or the whole brain. The corrected total cell fluorescence (CCF) = Integrated Density – (Area of selected cell X Mean fluorescence of background readings). The background was taken in the no-cell regions near the cell of interest.

Generation of plasmids and transgenic flies

Gateway® BP Clonase® II Enzyme mix (Invitrogen) was used for the generation of entry clone plasmids. cDNA clones were used in this study (*Drosophila* Genomics Resource Centre [DGRC]). Briefly, genes were amplified by polymerase chain reaction (PCR) first. Then, the amplified fragment was inserted into Gateway vector pDONR221 (Invitrogen) using Gateway BP Clonase II Enzyme mix to generate entry vector pDONR211-Pr-Set7. Subsequently, the fragment in the entry vector was inserted into Gateway destination vectors (pUAST) by LR recombination using Gateway LR Clonase II enzyme mix. The plasmids generated were pUAST-Pr-set7. Primers used for generating entry clones were as follows:

BP.Pr-set7.F: GGGG ACA AGT TTG TAC AAA AAA GCA GGC TTC ATGATAATGG TGCGAAGACG A.

BP.Pr-set7.R: GGGG AC CAC TTT GTA CAA GAA AGC TGG GTC TCAGAA GGCCAACCAA GGATG.

UAS-Pr-set7 transgenic flies were generated by standard P-element-mediated transformation by BestGenes, Inc.

Drosophila pr-set7 genomic constructs for genomic rescue

The selection criteria for bacterial artificial chromosomes (BACs) clone are to cover 10,000 bp upstream to 5,000 bp downstream of the genomic region of the gene (*pr-set7*). Therefore, *Pr-set7*-BAC (CH322-129L5) was obtained from the BACPAC Resources Center. To generate transgenic flies, the BAC clone was injected into stock BDSC#8621 yw; P{y[+7.7] = CaryP}attP1 (chromosome II, 55C4) based on Φ C31-integrase system by BestGene, Inc.

Generation of anti-Pr-set7 antibodies

The C-terminal coding sequence (encoding 412–691 amino acids) of Pr-set7 (Pr-set7-C) was amplified by PCR and inserted into the vector pMAL-c2X (In-Fusion HD Cloning Kit, Clontech). The expression of GST-Pr-set7-C was induced by isopropyl β -D-1-thiogalactopyranoside and purified by amylose resin (NEB). Purified MBP-Pr-set7-C was then injected into one guinea pig and one rabbit, and Pr-set7-C antibodies were generated and purified by GenScript (Hong Kong). Primers used for Pr-set7-C amplification are as follows:

Pr-set7.412-end.MBP.F: AGGATTTGAGAATTCCTGAACCAGCCAAA GCCACAA.

Pr-set7.412-end.MBP.R: TTGCCTGCAGGTTCGATCAGAAGGCCAACC AAGGATG.

Protein extraction and immunoblotting

Larval brains of proper genotype were dissected in PBS and homogenized in RIPA buffer (50 mM Tris pH 7.5, 150 mM NaCl, 1 mM EDTA, 1% Triton X-100, 0.5% sodium deoxycholate, 0.1% SDS) containing proteases inhibitors. The amount of brains needed depends on the size of the brain, protein level, and antibody quality. The protein extracts were separated by SDS-PAGE and analyzed by Western blotting.

Blots were probed with the following antibodies: mouse anti-Actin (1:5,000; MP Biomedicals, Cat#: 08691001), rabbit anti-GAPDH1 (1:5,000; GeneTex, Cat#: GTX100118), guinea pig anti-Pr-set7 (1:1,000; generated in this experiment), rabbit anti-Cdk1 (1:1,000; Millipore, Cat#: AB3241-25UL), and mouse anti-Arm (1:1,000; DSHB, Cat#: N2 7A1).

RNA extraction and qPCR analysis

Larvae were dissected in PBS, and RNA from brains was extracted using TRI reagent (Sigma-Aldrich) following the manufacturer's protocol. ProtoScript First Strand cDNA Synthesis kit (New England Biolabs, Inc.) was used for reverse transcription. qPCR was carried out with different primer pairs. The primers used are listed in Appendix Table S3. Results were analyzed using the REST excel file.

TaDa *in vivo* profiling analysis

To identify *in vivo* Pr-set7 target genes, full length of Pr-set7 was cloned into pUASTattB-LT3-NDam vector using In-Fusion HD Cloning Kit. pUASTattB-LT3-NDam was kindly provided by A. Brand. UAS-Dam-Pr-set7 (pUASTattB-LT3-NDam-Pr-set7) or UAS-Dam control (pUASTattB-LT3-NDam) was expressed under the control of the *grh*-Gal4 driver. Eggs were collected within a 6-h period and raised at 25°C for 24 h till larvae hatched out. Hatched larvae were transferred to 29°C for 24 h before dissection. Genomic DNA of Dam-Pr-set7 or Dam control was extracted and amplified as previously described (Ahn & Joyner, 2005). Around 1,500 larval brains were collected for each genotype. The Illumina TruSeq DNA PCR-free library preparation kit was used to construct libraries based on amplified DNA samples according to the manufacturer's protocol. The libraries were then sequenced on the Illumina MiSeq equipment. Paired reads (2 × 250 bp) were obtained from Dam-Pr-set7 or Dam control library and were aligned with *Drosophila melanogaster* (dm6) reference genome by Bowtie 2 (Langmead & Salzberg, 2012). The peaks were called by MACS (Zhang *et al*, 2008), and the nearby gene was annotated using HOMER (Heinz *et al*, 2010). From two biological replicates performed (namely Original and Replicate), 7,157 overlapping peaks (peak scores \geq 50) are listed in Appendix Table S1. 2,081 out of 2,876 peaks (72.4%) in the replicate sample were also present in the original set, suggesting the two biological replicates were well correlated.

Statistical analysis

Statistical analysis between two groups was performed by two-tailed Student's *t*-test or Mann–Whitney test, and a value of $P < 0.05$ was considered as statistically significant. For three groups and above, one-way ANOVA was performed and *P*-values are calculated. In this

work, ns (non-significant) indicates $P > 0.05$, * indicates $P < 0.05$, ** indicates $P < 0.01$, and *** indicates $P < 0.001$. All data were shown as mean \pm SD.

Data availability

Raw and processed sequencing data have been deposited into Gene Expression Omnibus (GEO) database under accession number GSE158764. The DamID data from this publication have been deposited to the Gene Expression Omnibus (GEO) database (<https://www.ncbi.nlm.nih.gov/geo/query/acc.cgi?acc=GSE158764>) and assigned the identifier GSE158764.

Expanded View for this article is available online.

Acknowledgements

We thank A Brand, F Matsuzaki, C. Doe, Y. Ahmed, J Skeath, the Hybridoma Bank, the Bloomington *Drosophila* Stock Center, Vienna *Drosophila* RNAi Center, *Drosophila* Genomics Resource Center (DGRC) for fly stocks, antibodies, and cDNA clones and Gao F. for technical assistance. This work is supported by the Duke-NUS Signature Research Program funded by the Ministry of Health (MOH-000143), Singapore (HW).

Author contributions

HW and JH conceptualized the data; JH, MG, QD, SYC, W-KS, SL, and PT performed methodology; JH and HW wrote the original draft; HW and JH reviewed and edited the manuscript; HW performed the funding acquisition and resources, and supervised the research.

Conflict of Interest

The authors declare that they have no conflict of interest.

References

- Ahn S, Joyner AL (2005) In vivo analysis of quiescent adult neural stem cells responding to Sonic hedgehog. *Nature* 437: 894–897
- Ayeni JO, Varadarajan R, Mukherjee O, Stuart DT, Sprenger F, Srayko M, Campbell SD (2014) Dual phosphorylation of cdk1 coordinates cell proliferation with key developmental processes in *Drosophila*. *Genetics* 196: 197–210
- Baig-Lewis S, Peterson-Nedry W, Wehrli M (2007) Wingless/Wnt signal transduction requires distinct initiation and amplification steps that both depend on Arrow/LRP. *Dev Biol* 306: 94–111
- Barski A, Cuddapah S, Cui K, Roh TY, Schones DE, Wang Z, Wei G, Chepelev I, Zhao K (2007) High-resolution profiling of histone methylations in the human genome. *Cell* 129: 823–837
- Beck DB, Oda H, Shen SS, Reinberg D (2012) PR-Set7 and H4K20me1: at the crossroads of genome integrity, cell cycle, chromosome condensation, and transcription. *Genes Dev* 26: 325–337
- Bellen HJ, Levis RW, Liao G, He Y, Carlson JW, Tsang G, Evans-Holm M, Hiesinger PR, Schulze KL, Rubin GM et al (2004) The BDGP gene disruption project: single transposon insertions associated with 40% of *Drosophila* genes. *Genetics* 167: 761–781
- Benchabane H, Xin N, Tian A, Hafler BP, Nguyen K, Ahmed A, Ahmed Y (2011) Jerky/Earthbound facilitates cell-specific Wnt/Wingless signalling by modulating beta-catenin-TCF activity. *EMBO J* 30: 1444–1458
- Bostock MP, Prasad AR, Chaouni R, Yuen AC, Sousa-Nunes R, Amoyel M, Fernandes VM (2020) An immobilization technique for long-term time-lapse imaging of explanted *Drosophila* TISSUES. *Front Cell Dev Biol* 8: 590094.
- Braun SM, Jessberger S (2014) Adult neurogenesis and its role in neuropsychiatric disease, brain repair and normal brain function. *Neuropathol Appl Neurobiol* 40: 3–12
- Britton JS, Edgar BA (1998) Environmental control of the cell cycle in *Drosophila*: nutrition activates mitotic and endoreplicative cells by distinct mechanisms. *Development* 125: 2149–2158
- Brunner E, Peter O, Schweizer L, Basler K (1997) pangolin encodes a Lef-1 homologue that acts downstream of Armadillo to transduce the Wingless signal in *Drosophila*. *Nature* 385: 829–833
- Brustel J, Tardat M, Kirsh O, Grimaud C, Julien E (2011) Coupling mitosis to DNA replication: the emerging role of the histone H4-lysine 20 methyltransferase PR-Set7. *Trends Cell Biol* 21: 452–460
- Bryja V, Cervenka I, Cajanek L (2017) The connections of Wnt pathway components with cell cycle and centrosome: side effects or a hidden logic? *Crit Rev Biochem Mol Biol* 52: 614–637
- Chell JM, Brand AH (2010) Nutrition-responsive glia control exit of neural stem cells from quiescence. *Cell* 143: 1161–1173
- Chen J, Rajasekaran M, Xia H, Kong SN, Deivasigamani A, Sekar K, Gao H, Swa HL, Gunaratne J, Ooi LL et al (2018) CDK1-mediated BCL9 phosphorylation inhibits clathrin to promote mitotic Wnt signalling. *EMBO J* 37: e99395
- Cheung TH, Rando TA (2013) Molecular regulation of stem cell quiescence. *Nat Rev Mol Cell Biol* 14: 329–340
- Clegg NJ, Whitehead IP, Williams JA, Spiegelman GB, Grigliatti TA (1993) A developmental and molecular analysis of Cdc2 mutations in *Drosophila melanogaster*. *Genome* 36: 676–685
- Colombani J, Raisin S, Pantalacci S, Radimerski T, Montagne J, Leopold P (2003) A nutrient sensor mechanism controls *Drosophila* growth. *Cell* 114: 739–749
- Congdon LM, Houston SI, Veerappan CS, Spektor TM, Rice JC (2010) PR-Set7-mediated monomethylation of histone H4 lysine 20 at specific genomic regions induces transcriptional repression. *J Cell Biochem* 110: 609–619
- Couture JF, Collazo E, Brunzelle JS, Trievel RC (2005) Structural and functional analysis of SET8, a histone H4 Lys-20 methyltransferase. *Genes Dev* 19: 1455–1465
- Cui K, Zang C, Roh TY, Schones DE, Childs RW, Peng W, Zhao K (2009) Chromatin signatures in multipotent human hematopoietic stem cells indicate the fate of bivalent genes during differentiation. *Cell Stem Cell* 4: 80–93
- Davidson G, Niehrs C (2010) Emerging links between CDK cell cycle regulators and Wnt signaling. *Trends Cell Biol* 20: 453–460
- Daynac M, Chicheportiche A, Pineda JR, Gauthier LR, Boussin FD, Mouthon MA (2013) Quiescent neural stem cells exit dormancy upon alteration of GABAAR signaling following radiation damage. *Stem cell research* 11: 516–528
- Daynac M, Tirou L, Faure H, Mouthon MA, Gauthier LR, Hahn H, Boussin FD, Ruat M (2016) Hedgehog controls quiescence and activation of neural stem cells in the adult ventricular-subventricular zone. *Stem Cell Reports* 7: 735–748
- Deng Q, Tan YS, Chew LY, Wang H (2020) Mspg governs acentrosomal microtubule assembly and reactivation of quiescent neural stem cells. *bioRxiv* <https://doi.org/10.1101/2020.01.24.918227> [PREPRINT]
- Ding R, Weynans K, Bossing T, Barros CS, Berger C (2016) The Hippo signalling pathway maintains quiescence in *Drosophila* neural stem cells. *Nat Commun* 7: 10510

- Ding WY, Huang J, Wang H (2020) Waking up quiescent neural stem cells: Molecular mechanisms and implications in neurodevelopmental disorders. *PLoS Genet* 16: e1008653
- Doetsch F, Garcia-Verdugo JM, Alvarez-Buylla A (1999) Regeneration of a germinal layer in the adult mammalian brain. *Proc Natl Acad Sci USA* 96: 11619–11624
- Faiz M, Sachewsky N, Gascon S, Bang KW, Morshead CM, Nagy A (2015) Adult neural stem cells from the subventricular zone give rise to reactive astrocytes in the cortex after stroke. *Cell Stem Cell* 17: 624–634
- Fodor BD, Shukeir N, Reuter G, Jenuwein T (2010) Mammalian Su(var) genes in chromatin control. *Annu Rev Cell Dev Biol* 26: 471–501
- Foley E, O'Farrell PH, Sprenger F (1999) Rux is a cyclin-dependent kinase inhibitor (CKI) specific for mitotic cyclin-Cdk complexes. *Curr Biol* 9: 1392–1402
- Foley E, Sprenger F (2001) The cyclin-dependent kinase inhibitor Roughex is involved in mitotic exit in *Drosophila*. *Curr Biol* 11: 151–160
- Gil-Ranedo J, Gonzaga E, Jaworek KJ, Berger C, Bossing T, Barros CS (2019) STRIPAK members orchestrate hippo and insulin receptor signaling to promote neural stem cell reactivation. *Cell Rep* 27: 2921–2933
- Heinz S, Benner C, Spann N, Bertolino E, Lin YC, Laslo P, Cheng JX, Murre C, Singh H, Glass CK (2010) Simple combinations of lineage-determining transcription factors prime cis-regulatory elements required for macrophage and B cell identities. *Mol Cell* 38: 576–589
- Huang J, Wang H (2018) Hsp83/Hsp90 physically associates with insulin receptor to promote neural stem cell reactivation. *Stem Cell Reports* 11: 883–896
- Isshiki T, Pearson B, Holbrook S, Doe CQ (2001) *Drosophila* neuroblasts sequentially express transcription factors which specify the temporal identity of their neuronal progeny. *Cell* 106: 511–521
- Ito K, Hotta Y (1992) Proliferation pattern of postembryonic neuroblasts in the brain of *Drosophila melanogaster*. *Dev Biol* 149: 134–148
- Karachentsev D, Sarma K, Reinberg D, Steward R (2005) PR-Set7-dependent methylation of histone H4 Lys 20 functions in repression of gene expression and is essential for mitosis. *Genes Dev* 19: 431–435
- Kawai H, Kawaguchi D, Kuebrich BD, Kitamoto T, Yamaguchi M, Gotoh Y, Furutachi S (2017) Area-specific regulation of quiescent neural stem cells by Notch3 in the adult mouse subependymal zone. *J Neurosci* 37: 11867–11880
- Ke X, Xing B, Yu B, Yu X, Majnik A, Cohen S, Lane R, Joss-Moore L (2014) IUGR disrupts the PPARgamma-Setd8-H4K20me(1) and Wnt signaling pathways in the juvenile rat hippocampus. *Int J Dev Neurosci* 38: 59–67
- Kim S, Ishidate T, Sharma R, Soto MC, Conte Jr D, Mello CC, Shirayama M (2013) Wnt and CDK-1 regulate cortical release of WRM-1/beta-catenin to control cell division orientation in early *Caenorhabditis elegans* embryos. *Proc Natl Acad Sci USA* 110: E918–927
- Kohlmaier A, Savarese F, Lachner M, Martens J, Jenuwein T, Wutz A (2004) A chromosomal memory triggered by Xist regulates histone methylation in X inactivation. *PLoS Biol* 2: E171
- Lai SL, Doe CQ (2014). Transient nuclear Prospero induces neural progenitor quiescence. *eLife* 3: e03363.
- Langmead B, Salzberg SL (2012) Fast gapped-read alignment with Bowtie 2. *Nat Methods* 9: 357–359
- Lee LA, Elfring LK, Bosco G, Orr-Weaver TL (2001) A genetic screen for suppressors and enhancers of the *Drosophila* PAN GU cell cycle kinase identifies cyclin B as a target. *Genetics* 158: 1545–1556
- Lee LA, Orr-Weaver TL (2003) Regulation of cell cycles in *Drosophila* development: intrinsic and extrinsic cues. *Annu Rev Genet* 37: 545–578
- Li S, Koe CT, Tay ST, Tan ALK, Zhang S, Zhang Y, Tan P, Sung WK, Wang H (2017) An intrinsic mechanism controls reactivation of neural stem cells by spindle matrix proteins. *Nat Commun* 8: 122
- Li Z, Nie F, Wang S, Li L (2011) Histone H4 Lys 20 monomethylation by histone methylase SET8 mediates Wnt target gene activation. *Proc Natl Acad Sci USA* 108: 3116–3123
- Lu X, Simon MD, Chodaparambil JV, Hansen JC, Shokat KM, Luger K (2008) The effect of H3K79 dimethylation and H4K20 trimethylation on nucleosome and chromatin structure. *Nat Struct Mol Biol* 15: 1122–1124
- Lucassen PJ, Meerlo P, Naylor AS, van Dam AM, Dayer AG, Fuchs E, Oomen CA, Czeh B (2010) Regulation of adult neurogenesis by stress, sleep disruption, exercise and inflammation: Implications for depression and antidepressant action. *Eur Neuropsychopharmacol* 20: 1–17
- Lugert S, Basak O, Knuckles P, Haussler U, Fabel K, Gotz M, Haas CA, Kempermann G, Taylor V, Giachino C (2010) Quiescent and active hippocampal neural stem cells with distinct morphologies respond selectively to physiological and pathological stimuli and aging. *Cell Stem Cell* 6: 445–456
- Ly PT, Tan YS, Koe CT, Zhang Y, Xie G, Endow S, Deng WM, Yu F, Wang H (2019) CRL4Mahj E3 ubiquitin ligase promotes neural stem cell reactivation. *PLoS Biol* 17: e3000276
- Mairet-Coello G, Tury A, DiCicco-Bloom E (2009) Insulin-like growth factor-1 promotes G(1)/S cell cycle progression through bidirectional regulation of cyclins and cyclin-dependent kinase inhibitors via the phosphatidylinositol 3-kinase/Akt pathway in developing rat cerebral cortex. *J Neurosci* 29: 775–788
- Morshead CM, Reynolds BA, Craig CG, McBurney MW, Staines WA, Morassutti D, Weiss S, van der Kooy D (1994) Neural stem cells in the adult mammalian forebrain: a relatively quiescent subpopulation of subependymal cells. *Neuron* 13: 1071–1082
- Nishioka K, Rice JC, Sarma K, Erdjument-Bromage H, Werner J, Wang Y, Chuiikov S, Valenzuela P, Tempst P, Steward R et al (2002) PR-Set7 is a nucleosome-specific methyltransferase that modifies lysine 20 of histone H4 and is associated with silent chromatin. *Mol Cell* 9: 1201–1213
- Oda H, Okamoto I, Murphy N, Chu J, Price SM, Shen MM, Torres-Padilla ME, Heard E, Reinberg D (2009) Monomethylation of histone H4-lysine 20 is involved in chromosome structure and stability and is essential for mouse development. *Mol Cell Biol* 29: 2278–2295
- Otsuki L, Brand AH (2017) The vasculature as a neural stem cell niche. *Neurobiol Dis* 107: 4–14
- Otsuki L, Brand AH (2018) Cell cycle heterogeneity directs the timing of neural stem cell activation from quiescence. *Science* 360: 99–102
- Otsuki L, Brand AH (2019) Dorsal-ventral differences in neural stem cell quiescence are induced by p57(KIP2)/Dacapo. *Dev Cell* 49: 293–300
- Otsuki L, Brand AH (2020) Quiescent neural stem cells for brain repair and regeneration: lessons from model systems. *Trends Neurosci* 43: 213–226
- Poon CL, Mitchell KA, Kondo S, Cheng LY, Harvey KF (2016) The hippo pathway regulates neuroblasts and brain size in *Drosophila melanogaster*. *Curr Biol* 26: 1034–1042
- Schotta G, Lachner M, Sarma K, Ebert A, Sengupta R, Reuter G, Reinberg D, Jenuwein T (2004) A silencing pathway to induce H3-K9 and H4-K20 trimethylation at constitutive heterochromatin. *Genes Dev* 18: 1251–1262
- Shi X, Kachirskaja I, Yamaguchi H, West LE, Wen H, Wang EW, Dutta S, Appella E, Gozani O (2007) Modulation of p53 function by SET8-mediated methylation at lysine 382. *Mol Cell* 27: 636–646
- Sousa-Nunes R, Yee LL, Gould AP (2011) Fat cells reactivate quiescent neuroblasts via TOR and glial insulin relays in *Drosophila*. *Nature* 471: 508–512
- Southall TD, Gold KS, Egger B, Davidson CM, Caygill EE, Marshall OJ, Brand AH (2013) Cell-type-specific profiling of gene expression and chromatin

- binding without cell isolation: assaying RNA Pol II occupancy in neural stem cells. *Dev Cell* 26: 101–112
- Speder P, Brand AH (2014) Gap junction proteins in the blood-brain barrier control nutrient-dependent reactivation of *Drosophila* neural stem cells. *Dev Cell* 30: 309–321
- Swarup S, Verheyen EM (2012) Wnt/Wingless signaling in *Drosophila*. *Cold Spring Harb Perspect Biol* 4: a007930
- Takawa M, Cho HS, Hayami S, Toyokawa G, Kogure M, Yamane Y, Iwai Y, Maejima K, Ueda K, Masuda A et al (2012) Histone lysine methyltransferase SETD8 promotes carcinogenesis by deregulating PCNA expression. *Cancer Res* 72: 3217–3227
- Talasz H, Lindner HH, Sarg B, Helliger W (2005) Histone H4-lysine 20 monomethylation is increased in promoter and coding regions of active genes and correlates with hyperacetylation. *J Biol Chem* 280: 38814–38822
- Trojer P, Li G, Sims III RJ, Vaquero A, Kalakonda N, Bocconi P, Lee D, Erdjument-Bromage H, Tempst P, Nimer SD et al (2007) L3MBTL1, a histone-methylation-dependent chromatin lock. *Cell* 129: 915–928
- Truman JW, Bate M (1988) Spatial and temporal patterns of neurogenesis in the central nervous system of *Drosophila melanogaster*. *Dev Biol* 125: 145–157
- Tsuji T, Hasegawa E, Isshiki T (2008) Neuroblast entry into quiescence is regulated intrinsically by the combined action of spatial Hox proteins and temporal identity factors. *Development* 135: 3859–3869
- Vakoc CR, Sachdeva MM, Wang H, Blobel GA (2006) Profile of histone lysine methylation across transcribed mammalian chromatin. *Mol Cell Biol* 26: 9185–9195
- Venken KJ, Schulze KL, Haelterman NA, Pan H, He Y, Evans-Holm M, Carlson JW, Levis RW, Spradling AC, Hoskins RA et al (2011) MiMIC: a highly versatile transposon insertion resource for engineering *Drosophila melanogaster* genes. *Nat Methods* 8: 737–743
- Wakabayashi K, Okamura M, Tsutsumi S, Nishikawa NS, Tanaka T, Sakakibara I, Kitakami J, Ihara S, Hashimoto Y, Hamakubo T et al (2009) The peroxisome proliferator-activated receptor gamma/retinoid X receptor alpha heterodimer targets the histone modification enzyme PR-Set7/Setd8 gene and regulates adipogenesis through a positive feedback loop. *Mol Cell Biol* 29: 3544–3555
- Wang YZ, Plane JM, Jiang P, Zhou CJ, Deng W (2011) Concise review: Quiescent and active states of endogenous adult neural stem cells: identification and characterization. *Stem Cells* 29: 907–912
- Wang Z, Zang C, Rosenfeld JA, Schones DE, Barski A, Cuddapah S, Cui K, Roh TY, Peng W, Zhang MQ et al (2008) Combinatorial patterns of histone acetylations and methylations in the human genome. *Nat Genet* 40: 897–903
- Wickramasekara RN, Stessman HAF (2019) Histone 4 lysine 20 methylation: a case for neurodevelopmental disease. *Biology (Basel)* 8: 11
- Wu S, Wang W, Kong X, Congdon LM, Yokomori K, Kirschner MW, Rice JC (2010) Dynamic regulation of the PR-Set7 histone methyltransferase is required for normal cell cycle progression. *Genes Dev* 24: 2531–2542
- Xiao B, Jing C, Kelly G, Walker PA, Muskett FW, Frenkiel TA, Martin SR, Sarma K, Reinberg D, Gamblin SJ et al (2005) Specificity and mechanism of the histone methyltransferase Pr-Set7. *Genes Dev* 19: 1444–1454
- Yan YP, Sailor KA, Vemuganti R, Dempsey RJ (2006) Insulin-like growth factor-1 is an endogenous mediator of focal ischemia-induced neural progenitor proliferation. *Eur J Neurosci* 24: 45–54
- Ye P, Popken GJ, Kemper A, McCarthy K, Popko B, D'Ercole AJ (2004) Astrocyte-specific overexpression of insulin-like growth factor-I promotes brain overgrowth and glial fibrillary acidic protein expression. *J Neurosci Res* 78: 472–484
- Yu Y, Liu L, Li X, Hu X, Song H (2019) The histone H4K20 methyltransferase PR-Set7 fine-tunes the transcriptional activation of Wingless signaling in *Drosophila*. *J Genet Genomics* 46: 57–59
- Zhang Y, Liu T, Meyer CA, Eeckhoutte J, Johnson DS, Bernstein BE, Nusbaum C, Myers RM, Brown M, Li W et al (2008) Model-based analysis of ChIP-Seq (MACS). *Genome Biol* 9: R137
- Zielke N, Korzelius J, van Straaten M, Bender K, Schuhknecht GFP, Dutta D, Xiang J, Edgar BA (2014) Fly-FUCCI: A versatile tool for studying cell proliferation in complex tissues. *Cell Rep* 7: 588–598
- Zouaz A, Fernando C, Perez Y, Sardet C, Julien E, Grimaud C (2018) Cell-cycle regulation of non-enzymatic functions of the *Drosophila* methyltransferase PR-Set7. *Nucleic Acids Res* 46: 2834–2849



License: This is an open access article under the terms of the Creative Commons Attribution-NonCommercial-NoDerivs 4.0 License, which permits use and distribution in any medium, provided the original work is properly cited, the use is non-commercial and no modifications or adaptations are made.